(24)

Characterizing the Influence of the General Circulation on Marine Boundary Layer Clouds

Margaret A. Rozendaal
Program in Earth and Environmental Sciences
Columbia University
New York, NY 10027

William B. Rossow
NASA Goddard Institute for Space Studies
New York, NY 10025

February 1, 2001

Submitted to Journal of the Atmospheric Sciences

Corresponding author address: Margaret A. Rozendaal
NASA/GISS
2880 Broadway
New York, New York 10025
E-mail: margaret@giss.nasa.gov

Abstract

The seasonal and intraseasonal variability of boundary layer cloud in the subtropical eastern oceans are studied using combined data from the International Satellite Cloud Climatology Project (ISCCP) and the European Centre for Medium-Range Weather Forecasts (ECMWF) reanalysis.

Spectral analysis reveals that most of the time variability of cloud properties occurs on seasonal to annual time scales. The variance decreases one to two orders of magnitude for each decade of time scale decrease, indicating that daily to monthly time scales have smaller, but non-negligible variability. The length of these dominant time scales suggests that the majority of the variability is influenced by the general circulation and its interaction with boundary layer turbulence, rather than a product of boundary layer turbulence alone.

Previous datasets have lacked the necessary resolution in either time or in space to properly characterize variability on synoptic scales; this is remedied by using global satellite-retrieved cloud properties. We characterize the intraseasonal subtropical cloud variability in both hemispheres and in different seasons. In addition to cloud fraction, we examine variability of cloud optical thickness - cloud top pressure frequency distributions. Despite the large concentration of research on the variability of Northern Hemisphere (NH) regions during summer, it is noted that the largest amplitude intraseasonal variability in the NH regions occurs during local winter.

The effect of intraseasonal variability on the calculation and interpretation of seasonal results is investigated. Decreases in seasonally averaged cloud cover, optical thickness and cloud top pressure from the May-through-September season to the November-through-March season are most apparent in the NH regions. Further analysis indicates that these

changes are due to an increase in frequency, but a decrease in the persistence of synoptic events. In addition, changes in cloud top pressure and optical thickness characteristics from the summer to winter seasons indicate that the NH subtropics undergo a change in dynamic regime with season. This change appears in the cloud fields as a shift from the more commonly seen lower-altitude, thicker optical thickness clouds to higher-altitude, thinner clouds. The latter cloud-type is associated with the lower sea level pressure, upward vertical velocity phase of the synoptic wave.

Intraseasonal changes in cloud properties in the Southern Hemisphere and NH summer are much smaller in amplitude. Although they also appear to be linked to changes in the large-scale dynamics, similarly to NH winter variations, the relationships are more ambiguous due to the small amplitudes and longer time scales. We attempt to interpret some of these relationships using the results of the Betts and Ridgway (1989) box model. However, these results cannot consistently explain the patterns when results from all regions are considered, implying that this model may not adequately explain all the processes involved in the variability.

I. Introduction

Surface and satellite observations (Warren et al. 1988; Rossow and Lacis 1990) show the eastern subtropical oceans to be covered primarily by low-level clouds confined to the boundary layer. Many mesoscale modelling studies focus on the role of boundary layer turbulence in the formation and dissipation of these clouds. In these cases, models generally simulate time periods of hours to days with fixed large-scale parameters (Moeng et al. 1995 and Bechtold et al. 1996 provide intercomparisons of some state-of-the-art mesoscale models). However, the geographical concentration of low clouds and an associated near-total absence of higher-level clouds imply that large-scale (and longer time scale) conditions exist which favor low clouds.

Global studies of low-cloud time variability have focused mainly on seasonal mean properties (Klein and Hartmann 1993 (hereafter KH93); Tselioudis et al. 1992) or seasonal variability of the diurnal cycle (Cairns 1995; Rozendaal et al. 1995; Bergman and Salby 1996). Studies of seasonal means note that some cloud and meteorological properties have their maxima during the northern hemisphere (NH) summer season, regardless of the local season. For instance, KH93 found a high correlation (r^2=0.88) between seasonally averaged surface-observed stratus cloud fraction and static stability for the months of June, July, and August (JJA) in both hemispheres. However, this relationship is less robust at intraseasonal time scales and for other months of the year (Klein et al. 1995; Klein 1997). Additionally, a physical mechanism linking low-cloud fraction and static stability has not been established, although a number of possibilities have been suggested (e.g. Randall 1980; Deardorff 1980; Slingo 1980; Klein 1994).

GCM studies have also concentrated primarily on seasonally averaged data. This lack of

intraseasonal information makes it difficult to identify sources of model deficiencies. For instance, some GCMs underestimate seasonal mean subtropical low-cloud fraction by 10-30% compared to surface observations (Del Genio et al. 1996; Ma et al. 1996) and the International Satellite Cloud Climatology Project (ISCCP - Jakob 1999). However, based on this information alone, it is impossible to tell whether these discrepancies are due to differences in frequency of occurrence or amount of coverage.

Comparisons between GCM and satellite-observed clouds on daily time scales highlight specific disagreements between the two. For instance, Webb et al. (1999) find that for one month of daily-averaged data in the Californian stratocumulus regime, three different GCMs show low clouds occurring less frequently than observed by ISCCP. Additionally, these GCM clouds are optically thinner than ISCCP with lower-altitude cloud tops. These differences can alter the radiation balance at the surface and therefore change the thermodynamics and dynamics of the boundary layer.

Recent experiments (Ma et al. 1996; Yu and Mechoso 1999; Gordon 2000; Li et al. 2000) artificially increase low-cloud fraction, persistence or optical thickness to study its effect on the radiation balance and SST of the eastern equatorial Pacific. For instance, in Ma et al. (1996), they assume that stratus clouds of a constant pressure thickness are present at all times over a portion of the tropical eastern ocean. This decreases both the solar radiation reaching the surface (by 100-150W/m^2) and the net upward LW radiation from the surface (by 70-90W/m^2). These changes allow model SSTs to cool by as much as 5°K compared to the control run, creating larger and more realistic latitudinal and longitudinal SST asymmetries, and thus increasing surface wind speeds and surface evaporation in the marine stratus regions.

Studies of time variability of marine low-level cloud on smaller spatial scales (summarized in Klein (1997)) have been restricted to the NH regions during summer, with most of the emphasis on the Californian region. In addition, many of these are limited to the examination of low-cloud fraction only. The types of variability studied include daily to monthly time scales in the Californian region (Klein 1997), the diurnal cycle (Simon 1977; Betts 1990; Blaskovic et al. 1992; Bretherton et al. 1995) and time variability in the vertical structure (Albrecht et al. 1995a; Norris 1998; Wang et al. 1999). The detail offered by these surface datasets is valuable for testing local correlations between clouds and their environment. However, these data cannot be used to examine the interactions of large-scale meteorology and clouds or to compare multiple regions during the same time period.

Previously, it was not possible to examine the synoptic variability of these clouds because datasets lacked the required resolution in either time (e.g. Warren et al. 1988) or space (individual weathership observations). These deficiencies are addressed here by combining satellite data and a model reanalysis product (observations interpolated by model output). Since this combination of information provides global coverage for all seasons, it is possible to compare the seasonal and intraseasonal variability of subtropical low clouds and their environment in several locations at once.

Section II describes the datasets, the model reanalysis product, and the details of some data analysis techniques used in this study. Section III describes the time variability spectrum for several cloud properties and identifies the seasonal cycle and the synoptic variability as the two most important scales of time variability. Similarities and differences in cloud properties for four subtropical regions are characterized on these scales. Section IV examines relationships between variability in cloud properties and the general circulation. We extend the analy-

sis of some known seasonal relationships between cloud and atmospheric variables and provide information on intraseasonal variability. Section V relates the NH wintertime intraseasonal variability of section IV to phases of synoptic scale waves. We also investigate the influence of changes in tropical convection on the seasonal and intraseasonal variability of subtropical low clouds. To do this, we compare patterns observed in our data to the predictions of a box model which specifically links changes in convective region variables to changes in subsiding regions.

II. Data

A. Satellite data

Nine years (1984-92) of data obtained from the ISCCP D-series (Rossow et al. 1996; Rossow and Schiffer 1999) are used in this analysis. The spatial resolution is 280 km (approximately 2.5°) and time resolutions are 3-hourly for the D1 series and monthly for D2. Since VIS/IR cloud information is only available for daylight hours, daily averages are calculated using these hours only. The data are not interpolated over the nighttime hours since the maximum and/or minimum values do not always occur during the daytime hours; therefore interpolation would not remove potential biases from the data. Biases and other errors in ISCCP VIS/IR cloud-top temperature and cloud fraction are discussed at length in Wang et al. (1999).

This study characterizes low clouds by examining the variability of cloud fraction, cloud optical thickness (TAU), and cloud-top pressure (CTP). Low-cloud is defined in ISCCP as having CTPs greater than 680mb. Upper-level cloud refers to all clouds with CTPs less than 680mb (middle + high-level cloud). Most of the results are presented for 10x10° domain sizes (boundaries given in Table 1); results for other domain sizes are included as necessary.

To be consistent with previous studies (e.g. Lau and Crane 1995, 1997; Tselioudis et al. 2000), TAU is used to describe cloud water changes rather than cloud liquid water path (LWP). However, these two variables are directly related at the smallest (pixel) scale for ISCCP water clouds by the relationship LWP = 6.292*TAU, where LWP is in g/m^2 when the effective droplet radius is 10 μm, (Rossow et al. 1996). A more detailed discussion of the relationship between the two variables can be found in Han et al. (1998). All analyses in this paper have been made using both variables; using LWP rather than TAU would not change our conclusions.

Although we generally use CTP to study variations in cloud-top location, occasionally we include information on cloud-top temperature (CTT) or cloud-top height (CTH). In this analysis, CTH is estimated as the difference between cloud-top and surface temperatures divided by a fixed lapse rate of 6.5 °K/km (e.g. Salby 1996). All tests in this paper were also performed substituting CTT or CTH for CTP. This substitution did not affect the conclusions so, unless otherwise noted, CTP is used as a proxy for either of these two variables.

The ISCCP dataset also includes atmospheric temperature and humidity information provided by the TIROS Operational Vertical Sounder (TOVS) product processed by NOAA NESDIS. In this study, precipitable water above the boundary layer (PW_{UP}) is defined as the sum of the TOVS precipitable water in the layers between 310 and 680mb. Static stability is calculated as the difference between the potential temperature at 740mb (θ_{740}) and the surface temperature. θ_{740} is calculated using the TOVS atmospheric temperature. Although a near-surface temperature is also available from TOVS, according to Figure 11 of Stubenrach et al. (1999), TOVS temperatures over these regions tend to run approximately 2°K colder at the surface and 0-1°K warmer at 740mb compared to 3I sounding data. Therefore, we try to

minimize this systematic error by using the mean surface skin temperature from the ISCCP clear-sky composite to represent the surface temperature (Rossow et al. 1996; Rossow and Schiffer 1999).

B. ERA-15

Meteorological variables are provided by the European Centre for Medium-Range Weather Forecasts Reanalysis level III-B surface and upper air data for 1979-1993 (known as ERA-15, hereafter ERA). We extract model products for the same time and spatial resolution as the ISCCP data, except that daily averages are calculated using 6-hourly model data.

This study uses ERA sea level pressure (SLP) from the surface dataset, plus temperature (T), specific humidity (S), zonal wind speed (U), meridional wind speed (V) and vertical pressure velocity (ω) at various pressure levels indicated by a subscript (for instance, V_{1000} is the meridional wind speed at 1000mb). ERA static stability is calculated as the difference between potential temperatures at 700 and 1000mb (θ_{700}-θ_{1000}). Vertical shear of the zonal wind speed (U_{shear}) is represented by U_{500}-U_{1000}. The meridional change in any variable across the region is estimated as the difference between the equatorward most and poleward most boxes (X_{eq}-X_{pole}) within the 10x10° domain, at the longitude farthest away from the coast. The zonal change is estimated as the difference between the box closest to the coast and the one farthest from the coast (X_{coast}-X_{ocean}) within the 10x10° domain, at the latitude closest to the equator. The subscripts "u" and "v" are used to designated zonal and meridional changes respectively, for instance, "Δ_vSLP" represents the meridional change in sea level pressure across the domain.

C. Ocean weathership sounding data

This study uses upper air data from Ocean Weatherships N (ship N - 30N, 140W) and

P (ship P - 50N, 130W). We limit the data to the nighttime hours due to daytime biases in temperature and relative humidity (e.g. Klein 1997; Norris 1998). Sounding data are available for the years of 1949-1974 for ship N and 1949-1970 for ship P. These soundings provide vertical profiles of pressure, height, temperature and relative humidity at 50mb intervals. We use the relationships outlined in Bolton (1980) to convert the data to water vapor mixing ratio (q), potential temperature (θ), and equivalent potential temperature (θ_e) as necessary.

We identify the pressure and temperature associated with the base of the temperature inversion using the method described in Klein (1997). Since the temperature inversion is associated with a rapid increase in temperature and decrease in relative humidity with height, these differences are calculated for each 50mb layer. However, since these changes can occur in layers less than 50mb in thickness, the inversion structure may not appear explicitly in these coarse resolution soundings. Instead, it is assumed that the layer containing the inversion will show the smallest fall in temperature and the largest decrease in relative humidity with height. If these changes occur in the same layer, then the base of the trade inversion is marked as the pressure at the base of this 50mb layer. Soundings which do not meet both of these criteria are discarded from the analysis.

D. Data compositing method

Similar to earlier studies of this kind (Klein et al. 1995; Klein 1997; Lau and Crane 1995, 1997; Tselioudis et al. 2000; Norris and Klein 2000), we composite ISCCP cloud properties in categories based on anomalies in meteorological data from ERA. In particular, we follow the method of Tselioudis et al. (2000) who use 12-hourly SLP anomalies to identify the passage of low-pressure systems and to group clouds by synoptic regime.

In order to concentrate on time variability, the data are spatially averaged over 10x10°

regions. A time series of anomalies is constructed by subtracting monthly means from daily averages. These anomalies are separated into May-September (MJJAS) and November-March (NDJFM) seasons and are referred to as "seasonal anomalies" through the rest of this paper. For each season, the resulting anomalies are separated into positive and negative groups and the median value is calculated for each group. All of the anomalies, and their associated cloud properties, are then resorted into three groups: anomalies larger than the positive median (POS ANOM), anomalies less than the negative median (NEG ANOM) and anomalies larger than the negative median, but smaller than the positive one (ZERO ANOM) (see Figure 1 of Tselioudis et al. 2000 for an illustration).

Sometimes changes in cloud property regimes more strongly related to changes in actual values of meteorological variables rather than the anomalies. In these cases, the 25 and 75% quantile values of the meteorological data are calculated and cloud properties are sorted into three groups based on where the associated meteorology falls on the frequency distribution: actual values larger than the 75% quantile, values between the 25 and 75% quantiles and values below the 25% quantile.

When discussing CTP-TAU frequency distributions, we generally refer to the 6 TAU classes and 7 CTP classes defined in Figure 2.5 of Rossow et al. (1996) and used by Tselioudis et al. (2000). When discussing smaller magnitude changes, the number of classes is increased to 12 TAU (with boundaries at 0.02, 0.5, 1.27, 2.3, 3.55,6.0, 9.38, 14.5, 22.63, 34.74, 60.36, 109.8, and 378.65) and 14 CTP (with boundaries at 1000, 900, 800, 740, 680, 620, 560, 500, 440, 375, 310, 245, 180, 105 and 30 mb).

III. Characterizing subtropical cloud variability

A. Variability spectrum

Using four of the subtropical domains chosen by KH93 (Table 1), we calculate the power spectra for TAU, CTP and cloud fraction. This spectral method uses five overlapping windows, with 512 days in each window (the method requires the window size to be a power of two). The power spectrum of total cloud TAU in Figure 1 shows the dominance of seasonal to annual time scales in temporal cloud variability (the spectra for cloud fraction and CTP are similar and therefore not shown). The spectra for low-cloud TAU and cloud fraction show an even larger concentration of power at these longer time scales. The shape of the spectrum is clearly "red" (e.g. Gilman et al. 1963), so most of the variance occurs at longer time periods. The power decreases one to two orders of magnitude for each decade of time scale decrease, but there is a plateau at weekly to monthly time scales. The existence of the plateau indicates that not all of the power at daily to monthly time scales is cascading down from longer time scales, but that a source must exist to inject energy into the system near these time scales. Since both the temporal and spatial spectra (e.g. Pandolfo 1993; Rossow and Cairns 1995) are red in character, longer time scales tend to be associated with larger spatial scales. The length of the dominant time scales indicates that the majority of the cloud variability is influenced by the general circulation and its interaction with boundary layer turbulence, rather than the local product of boundary layer turbulence alone.

Since the data are daily averages, there is no spectral information for periods less than the Nyquist frequency of 2 days. Using a cutoff of $1/e \sim .37$ for the autocorrelation, the decorrelation time scale for total cloud TAU, CTP and cloud fraction is about 3 days in all regions. The temporal power below one day is not known from these data, but studies at higher spatial resolution show that the spatial power spectrum for stratocumulus clouds continues to follow a power law relationship (Welch et al. 1988; Sengupta et al. 1990) and that the magnitude of

cloud variations at scales smaller than approximately 5km contributes little to the total cloud variability (Barker 1996; Chambers et al. 1997). Given these results and the negative slopes of both the time and spatial power spectra, the variance continues to decrease at shorter time scales. Therefore, there is more power at the few-days to seasonal time scales than at the hourly-daily time scales characteristic of boundary layer turbulence.

We test the dependence of spectral shape on changes in the size of the averaging domain, latitude and longitude, and season. As the domain size increases from 2.5x2.5° to 20x20°, more power is found at seasonal to annual time scales and less at intraseasonal. This is not unexpected since shorter period variability is smoothed by spatial averaging as the domain size increases. Varying the location of several 5x5° boxes within the larger 20x20° domain causes small changes in power at the seasonal frequencies and slight changes in slope between the seasonal and intraseasonal frequencies. However, no major differences in spectral shape were noted. If the spectrum is calculated for MJJAS and NDJFM separately, the NH regions exhibit some changes in shape with season. During NDJFM, there is an increase in power at intraseasonal time scales for periods less than 30 days, and a decrease in the slope between seasonal and intraseasonal time scales. In contrast, the southern hemisphere (SH) regions show no significant changes in power or spectral shape with season. The differences in variability between hemispheres will be explored in later sections.

B. Seasonal variability

We extend previous studies of the seasonal variation of low-cloud fraction to include the variations of other cloud properties as well as variations in the ISCCP cloud-types (Table 2). As noted in earlier papers (e.g. Schubert et al. 1979; KH93), seasonally averaged low-cloud fraction is larger during MJJAS than NDJFM in all of these eastern ocean subtropical regions,

regardless of whether the local season is summer or winter. The MJJAS upper-level cloud fraction is smaller, around 10%, with most of the coverage by middle cloud. Therefore, the possibility of obscuration of low-level cloud by upper-level cloud is rare during this season.

When subdivided by cloud-type, most of the low-cloud falls into the "stratocumulus (Sc)" TAU category, in the range of 3.6 to 23.3 (Rossow et al. 1996). 70-75% of the VIS/IR low-cloud fraction is Sc and 17-25% cumulus (Cu) with smaller amounts of stratus (St) in all regions except the Canarian. The low-cloud fraction in the Canarian region is comprised of almost equal parts Sc and Cu. These differences in low-cloud fraction amount and type among the subtropical regions are in qualitative agreement with seasonally averaged surface observations from the Ocean Cloud Atlas (Warren et al. 1988), despite differences in the definition of these cloud-types for each dataset. Hahn et al. (2001) provide a comprehensive discussion of the extent to which ISCCP clouds are associated with standard surface observer cloud-types. To summarize, ISCCP cannot distinguish between Cu, Sc and St cloud-types in individual observations because of the considerable overlap in the CTP-TAU distributions associated with each of these cloud-types. However, changes in ISCCP TAU resemble expected changes in surface-observed cloud-type when surface observations are composited into spatial and seasonal averages. Therefore, in this section, we treat surface-observed and ISCCP cloud-types as though they are equivalent; but in later sections, when we examine distributions of daily averaged data, we refer to clouds of different TAU as "thinner" and "thicker" clouds.

During NDJFM, low-cloud fraction decreases in all regions relative to the MJJAS values. This is primarily a decrease in Sc type cloud fraction; changes in Cu and St cloud fractions are of mixed sign. Part of this decrease may be caused by an increase in obscuration by

upper-level cloudiness, but with the exception of the Canarian region, low-cloud fraction decreases are larger than increases in upper-level cloudiness. From these data alone, it is impossible to determine the extent to which upper-level clouds replace or obscure low-level clouds. However, this seasonal decrease of low-cloud fraction is consistent with results from the Ocean Cloud Atlas. In this case, the surface-observed decrease in low-cloud fraction is the result of decreases in coverage by St and Sc cloud types and increased coverage by Cu.

Low-cloud TAU and CTH are calculated for the low clouds that are seen. The relationship between seasonal variations in TAU and atmospheric temperature appears to be inconsistent with Tselioudis et al. (1992) since low-cloud TAU is larger during locally warm seasons. However, as pointed out in their paper, this relationship is very sensitive and averaging over eight years of data as well as several months of the year includes time periods where the relationship changes sign. When subdivided by cloud-type, TAU values for Cu and Sc cloud-types are larger in MJJAS, while St TAUs are smaller during this season. Therefore, as the season changes from MJJAS to NDJFM, thicker clouds increase in thickness while thinner clouds become thinner.

We find that seasonal changes occur in the classification of low clouds by ISCCP. In the MJJAS season, the VIS/IR scheme reports larger cloud fractions than the IR-only scheme for all cloud-types in all regions. During NDJFM the situation is reversed, with the IR-only scheme reporting more low-cloud cover than the VIS/IR. Since the IR scheme alone can never "see" more clouds than the combined VIS/IR scheme, this is due to a reclassification of low-level cloud as mid-level cloud. In the IR detection scheme, clouds are assumed to be opaque to IR radiation. If the VIS/IR scheme determines that a cloud is optically thin, the CTP is recalculated, placing the cloud-top at a higher altitude in the atmosphere. In our anal-

ysis of intraseasonal variability, we consider variations in total cloud properties, rather than low-cloud alone, to avoid discarding these mid-level clouds.

Low-cloud CTH is smaller during MJJAS in all regions except the Namibian. The definition of CTH (given in the data section) is important because the apparent increase in mean low-cloud CTH in NDJFM occurs for different reasons in different hemispheres. While both cloud-top and surface temperatures are warmest in local summer, mean NH cloud top temperatures decrease by more than mean surface temperatures as the season shifts from summer to winter. In contrast, during NDJFM, SH surface temperatures increase by more than cloud top temperatures. This implies that variability in the SH properties could occur on longer time scales and lag behind changes in the NH since atmospheric temperatures change on shorter time scales than SSTs. Indeed, for low-cloud fraction and CTH, larger correlations are found between monthly mean NH and SH data if the SH values are lagged behind the NH by 1-2 months. The fact that the cloud properties tend to change in similar ways in the same calendar months rather than local season also points to large-scale circulation controls on subtropical cloud variability.

C. Intraseasonal variability

1. Changes in frequency and persistence with season

Although the dominance of seasonal to annual periods in the temporal power spectra of low-cloud fraction, TAU and CTP justifies the concentration of effort on seasonal variability, intraseasonal data is used to examine relationships between synoptic meteorology and cloud variables. Figure 2 shows a time-longitude Hovmoller diagram for low-cloud fraction at latitudes of 25-30°N (Californian). From approximately May to September, fairly stationary and persistent large low-cloud fraction events are readily apparent. The events are not regu-

larly spaced in time nor do they persist for the same length of time. The same is seen in the Peruvian and Namibian regions (not shown). However, as also noted in KH93, the initiation of large low-cloud fraction events in these regions lag behind the Californian by one to two months.

During this season, the characteristics of cloud properties in the Canarian region are different from the other three subtropical regions. The time-longitude diagram of all cloud properties, but particularly CTP (not shown), indicates that upper-level cloud events propagate from east to west at estimated speeds of 10m/s and, by obscuring or replacing the lower-level clouds, shorten the perceived low-cloud persistence.

For the other months of the year, the persistence and propagation characteristics of the synoptic variability change. In the SH, large low-cloud fraction events decrease in both magnitude and frequency, but are still stationary. In the NH regions, the persistence and frequency of occurrence of large low-cloud fraction events is similar to the Canarian MJJAS variability, except that the upper-level cloud events propagate in the other direction, from west to east.

We quantify these observations by counting the number of times low-cloud fraction exceeds a chosen threshold value, and once it does, how many days it remains above this value. For a threshold value of 70%, Table 3 shows that large low-cloud fraction events occur more frequently during MJJAS in all regions except the Canarian. This exception occurs because low-cloud fraction in the Canarian region seldom reaches 70%; but the same result is achieved there when the threshold value is reduced to 50%. Figure 3 shows that in the NH regions, not only is the frequency of occurrence of these large events greater during the MJJAS season, but so is the average persistence of individual events. The persistence in the SH regions is approximately the same in both seasons.

In contrast to the seasonally averaged picture, large low-cloud fraction events appear in both seasons, but they occur more often and last for a shorter period of time in the NH during winter. Therefore, observed seasonal differences in low-cloud fraction are due primarily to changes in mean values in the SH and to changes in frequency of occurrence and persistence in the NH.

2. Changes in the intraseasonal cloud property frequency distribution with season

Although the seasonal average is a commonly reported statistic, other characteristics of a distribution are often more informative, particularly if the distribution shape is not normal. For low-cloud fraction (Figure 4) and total cloud fraction (not shown) the shape of the frequency distribution varies with domain size. At the 2.5x2.5° spatial scale, the distributions have a wide range of mode values, varying from 20% in the Canarian region to nearly overcast in the Namibian. The mode values converge to approximately 60% and the shape of the distribution approaches near normal as the domain size increases to 20x20°. This is consistent with observations of Rossow and Cairns (1995) and Klein (1997) for subtropical surface observations. Both demonstrate that the cloud fraction frequency distribution is dominated by completely overcast or clear-sky cases at smaller spatial scales, but the mode value approaches partly cloudy as the domain size increases. Therefore, in Table 2, the apparent similarity of seasonally averaged low-cloud fractions between regions masks different types of intraseasonal variability.

In contrast to cloud fraction, frequency distributions for total cloud TAU (Figure 5) and CTP (not shown) exhibit little variation in shape or mode with averaging domain size. These distributions are monomodal, with the distribution becoming narrower as the domain size increases. This occurs primarily because TAU and CTP variables are undefined under

clear-sky conditions, therefore these scenes are omitted from the distributions (Rossow and Cairns 1995).

Figure 6 characterizes subtropical clouds using the two dimensional frequency distribution of total cloud TAU and CTP for the 10x10° domain (results are similar on all spatial scales). During MJJAS, the Californian distribution looks more like the SH distributions, with primarily low-altitude cloud tops and a broad range of TAU values. Cloud properties in the Canarian region are distributed differently, with more frequently occurring high-altitude cloud tops and lower TAU values. As the season shifts from MJJAS to NDJFM, the most drastic change in cloud properties occurs in the Californian region, where the frequency of occurrence increases for higher-topped clouds and decreases for larger TAU clouds.

The differences in persistence, propagation and cloud-type between seasons indicate a shift in dynamic regime in the NH subtropics. The NH regions are located more poleward than their SH counterparts (see Table 1). This latitudinal difference, combined with an equatorward shift in NH storm-track activity during the NH winter season (Trenberth 1991; Rossow et al. 1993) allows midlatitude storms to intrude into the NH subtropical regions. In contrast, the SH regions do not show this change in variability since the storm-track is located at approximately 45°S all year around, keeping the storms poleward of the subtropical stratiform cloud regions. The effect of synoptic storms on low-cloud variability in the subtropics are explored further in the following sections.

IV. Subtropical cloud and the general circulation

A. Seasonal cycle

1. Exploring the correlation between subtropical low-cloud fraction and static stability

Previous studies found a significant correlation between the variability of large-scale

meteorology and cloud on seasonal and intraseasonal time scales, in particular, a large correlation exists between seasonal variations in surface-observed low-cloud fraction and lower tropospheric static stability (KH93). Since the coefficient is so large, this relationship is sometimes used in models to simulate the seasonal cycle of subtropical low-cloud (e.g. Philander et al. 1996; Miller 1997; Clement and Seager 1999; Larson et al. 1999).

However, as discussed in KH93, this correlation is calculated using seasonally averaged data at many locations (Figure 13 of KH93). In this diagram, geographic variations in stability between locations during one season are of the same magnitude as seasonal variations taken at one location for many seasons. Therefore, it is not clear how much of this large correlation is due to correlation in time and how much to correlation in space. Although the time-series of seasonally averaged stability and cloud fraction imply that the seasonal correlation is probably large, we would like to test the time dependence of this statistic separately.

Are the correlation coefficients still large if the calculation is made for each region separately? We address this question by creating seasonal anomalies for low-cloud fraction and static stability (by removing the annual average from the seasonally averaged data), and then calculating the slope and correlation coefficient for a best-fit line to a scatterplot of the anomalies (Table 4). The resulting slopes are consistently less than KH93 and the correlation coefficients range from fair to good, but are never as large as theirs. If we assume that the reason for this disagreement is that ISCCP is missing low clouds due to obscuration by higher clouds, then a correction can be estimated by altering the cloud amounts with a random overlap assumption (e.g. Rozendaal et al. 1995) or a maximum overlap assumption (all upper-level cloud has low-level cloud beneath it). However, a correction of this kind should actually decrease, rather than increase, the slope of the best-fit line, since it would presumably increase

the "smaller" low-cloud fraction values. This hypothesis is confirmed by Table 4, which shows that coefficients and slopes for corrected low-cloud fraction decrease in the NH (particularly for maximum overlap), but do not change by much in the SH. Therefore, these corrections do not improve the agreement with KH93.

What is the difference between the seasonal cycle of low-cloud fraction predicted by KH93 and the cycle predicted using the best-fit line at each location? In this case, the relationship of KH93 and static stability anomalies are used to predict the seasonal cycle of low-cloud fraction. The result is then correlated with seasonal anomalies in ISCCP low-cloud fraction (not shown). In this case, the closer the slope and correlations coefficients are to one, the better stability is as predictor of the seasonal cycle. In general, the correlation coefficients are slightly lower than in the previous case. This implies that using the global relationship of KH93 does not enable us to predict the seasonal cycle of low-cloud fraction at an individual location more accurately than if we fit the data separately at each location. In addition, the correlation coefficient calculated by fitting data from all regions is larger the ones calculated for each region separately, indicating that some of the KH93 correlation may be due to spatial rather than seasonal variability.

The analysis above shows some of the limitations of using stability as a seasonal predictor of low-cloud fraction, but it does not move us any closer to establishing why static stability ought to be related to low-cloud cover. Klein (1994) rules out the idea of low clouds changing static stability since clouds do not appear to affect heating rates in the upper atmosphere (and therefore θ_{740}) and the time scale for changing SST is on the order of a few months. (In our study, we are using surface temperature rather than SST, but daily observations are still autocorrelated for two to three months). He proposes that changes in stability

could cause changes of low-cloud cover either through cloud-top entrainment instability or changes in inversion height. Although these mechanisms have been examined (Klein et al. 1995; Klein 1997), no conclusive evidence has been established. This leaves a third possibility: that changes in stability and low-cloud amount are both modified by the large-scale circulation and that their may not be a direct link between stability and cloud cover.

2. Exploring lagged correlations between tropical and subtropical cloud properties

Theories connecting seasonal changes in subtropical low-cloud properties to variations in tropical convection are not very specific about the physical mechanism linking the two. Several have suggested a link between increasing tropical convection and increasing area coverage by marine stratocumulus clouds. Schubert et al. (1979) assert that "areas of marine stratocumulus convection are most extensive in the Northern Hemisphere summer, when the upward motion in the ITCZ and the downward motion in the subtropical highs is strongest". This idea seems contrary to GCMs experiments which show that the mass flux in the descending branch of the Hadley cell is actually strongest in the wintertime hemisphere (e.g. Rind and Rossow 1984; Hack et al. 1989). This is supported by Philander et al. (1996), who find poor correlations between changes in subsidence and cloudiness. KH93 suggest that the strength of the subtropical inversion is likely tied to the strength of the Hadley Cell and the amount of deep convection in the tropics. In theory, if SST is held constant, an increase in subsidence could increase the subtropical temperature inversion strength through the adiabatic warming of descending air.

Studies attempting to link the two regions focus on longer time scale variability associated with climate change. Several box model studies test the response of low-cloud properties in tropical subsidence regions to changes in convective properties in the tropics (Sarachik

1978; Betts and Ridgway 1989 (hereafter BR89); Miller 1997; Clement and Seager 1999; Larson et al. 1999). In these cases, some of the cloud properties are specified or parameterized.

We observe in time-longitude plots of daily average CTP (not shown) and in seasonal averages (Table 2), that eastern subtropical CTPs tend to be larger and more spatially homogeneous during the MJJAS season. In this same season, the ITCZ (as represented by ISCCP CTP) has smaller CTP values, covers a narrower range in latitude, and is located at its northernmost position. A similar pattern is seen in Mitchell and Wallace (1992), who note that as the ITCZ shifts northward, SSTs drop over the cold tongues, perhaps in response to the decrease in solar radiation reaching the sea surface as the coverage of low-cloud increases. However, this relationship has a feedback aspect as demonstrated by Chang and Philander (1994), who find that their GCM has difficulty correctly locating the ITCZ in the NH without low clouds to aid in cooling of subtropical SSTs.

Regardless of which is the cause and which is the effect, we express these observations quantitatively as a change in the shape of the distribution of CTP within selected regions of the subtropical and tropical Pacific (boundaries for the subtropical regions are given in Table 1; the tropical regions in Table 5). The boundaries of the tropical domains are selected to accommodate seasonal shifts in latitude of the ITCZ. Since tropical convective clouds only occupy a small portion of this domain at any given time, we examine changes in the spatial standard deviation of CTP over the entire box, rather than changes in the mean CTP. As tropical convective clouds become particularly high-altitude and coherent, the spatial standard deviation of CTP (STD_{CTP}) over the domain increases (since the remaining portion of the region is covered by lower-level clouds).

In the tropics, the amount of deep convective cloud cover (DCC) is a strong control on

the STD_{CTP}; as the amount of high-level cloud increases, the standard deviation increases (as the number of small CTP values in the tail of the CTP frequency distribution increases). This is true for standard deviations calculated over time and space. DCC is moderately to well-correlated (r values between than 0.42 to 0.56 for the Pacific regions in Table 5 with significance at the 99% level) with STD_{CTP} in the tropical regions; therefore, we interpret an increase in STD_{CTP} as an increase in the area covered by convective cloud. In the subtropics, STD_{CTP} has a strong negative correlation with low-cloud fraction (with r values of -0.90 and -0.75 with significance at the 99% level), so a decrease in STD_{CTP} is interpreted as an increase in the area covered by low-cloud.

Based on these interpretations, we expect that if increasing DCC in the tropics is related to increasing coverage by lower-level clouds with larger, more homogeneous CTPs in the subtropics, STD_{CTP} in these two locations will be negatively correlated. Time series of STD_{CTP} (Figure 7a) show a well-defined seasonal cycle in the spatial variability of CTP in all regions. Given its cyclic nature, it is impossible to tell for certain which peaks constitute the lead effect and which are the lagged result. However, given our hypothesis, we assume that the large STD_{CTP} values in the tropics (increasing DCC) lead the small STD_{CTP} values in the subtropics (increasing low-cloud cover).

Correlations among the tropical regions show that maximum STD_{CTP} values occur first in the eastern Pacific, and then in the western Pacific 2-3 month later (the same lag is observed directly for DCC in the tropics). If the connection between changes in variability in the tropics and subtropics is direct, then the lag time between observed tropical variability and the subtropical response should increase from east to west.

Correlations between the subtropics and the eastern Pacific are negative and largest in

magnitude if the Californian region (Figure 7b) lags the tropical region by 1 month and Peruvian (not shown) lags by 2-3 months. When we extend this analysis to include the western Pacific, the lagged relationships are not what we expect given our hypothesis. Lagged correlations coefficients between the Peruvian region and the western Pacific are larger in magnitude than correlations with the eastern Pacific, and the lag time is reduced to 1 month. This would imply that the Peruvian region responds more rapidly to a change in convection in the western Pacific than to a change in the eastern Pacific. In this case, the Californian actually lags the western Pacific by up to 10 months.

There are several ways that an increase in the areal coverage of tropical convective clouds could influence the subtropics. One idea is that an increase in the amount of tropical convection could cause the air above the inversion to become more moist. According to box model experiments, increasing the specific humidity above the boundary layer would cause the inversion height in the subsidence region to decrease because radiative cooling decreases (e.g. BR89; Miller 1997, Larson et al. 1999). However, although boundary layer clouds have larger seasonally averaged CTPs during MJJAS, the SH regions have a seasonal minima in upper-level specific humidity (given either by ERA S_{700} or TOVS PW_{up}).

A second possibility is that increasing convection in the tropics causes upper tropospheric temperatures to warm, which increases the large-scale static stability. This could limit the mixing of drier air from above the boundary layer and the vertical propagation of moist plumes from below. However, Philander et al. (1996) notes that seasonal changes in static stability occur for different reasons in different hemispheres; the NDJFM decrease occurs due to large decreases in θ_{740} in the NH, but due to increases in surface temperatures in the SH. Therefore, although a seasonal relationship between stability and low-cloud fraction does

exist, this cannot consistently explain the change in stability in both hemispheres.

A third possibility is that stronger subsidence rates during the MJJAS season in the subtropics, driven potentially by a larger area of vertical updrafts in the tropics, cause larger subtropical CTPs because more dry air mixes across the inversion into the boundary layer. However, in all regions, seasonally averaged ERA ω_{700} is always larger during local winter, consistent with Rind and Rossow (1984). Therefore, this possibility does not seem to be true for the NH regions.

If data from subtropical regions in both hemispheres is considered, none of these proposed mechanisms consistently explains the seasonal variability. In addition, the variability explained by correlations between subtropical and individual tropical regions is only 25-30%. If the tropical regions are added one by one in a multivariate correlation analysis with the subtropics, the explained variability can be increased to approximately 45%, but this still leaves about half the variance unexplained. Therefore, we turn to intraseasonal variability to try to better understand the patterns seen in seasonal averages.

B. Intraseasonal variability of subtropical cloud and the general circulation

Thus far, studies of low-cloud fraction data have found no single good predictor of submonthly cloud fraction variability. Correlations between low-cloud fraction and some large-scale meteorological factors on the synoptic time scale are examined by Wylie et al. (1989) for FIRE and by Klein (1997) during the MJJAS season at ship N. These studies show increases in low-cloud fraction with increases in cold, dry advection, wind steadiness, latent heat flux, SLP and surface divergence. However, the correlation coefficients are small, with r values no larger than 0.35. In theory, an increase in cold, dry advection increases the sensible and latent heat fluxes between the relatively warm, moist ocean surface and the overlying air.

An increase in surface wind speed also increases the magnitude of surface heat fluxes, and in addition, creates stronger wind shear which increases the mechanical stirring in the near-surface boundary layer. One possible reason that these coefficients are so small is that the surface-observed cloud data are point measurements rather than truly synoptic in spatial scale. Increasing the size of the averaging domain can increase the effective number of independent samples and decrease the standard error of the estimates if the averaging region is large compared to spatial correlation lengths of a few thousand kilometers (Leith 1973).

However, if we repeat the calculations mentioned above and increase the spatial scale of the data by using ISCCP and ERA data on the 10x10° domain, the magnitude of the correlations coefficients does not increase. In addition, if we repeat our earlier analysis for seasonally averaged low-cloud fraction and stability with daily anomalies (the seasonal mean removed), the magnitude of the r correlation coefficients decreases to less than 0.4 for all regions in either season. Klein et al. (1995), in their study of interannual variability, increase their correlation coefficients by lagging the time-series by a day or two; this does not increase the coefficients in our case.

In the NH regions, power spectra for static stability, surface temperature and θ_{740} (not shown) have a factor of two more power at seasonal to annual time scales (roughly 90 days to one year) than cloud fraction, TAU or CTP. In addition, these variables are autocorrelated for longer periods than cloud variables. Therefore, since temperature variables have more "memory" than cloud variables, their variability alone may not be a good proxy for submonthly low-cloud variability.

We mentioned previously that changes in the intraseasonal variability of clouds in the NH from summer to winter indicates a change in dynamic regime with season. This shift is

quantified in the meteorological variables as an increase in the range and standard deviation of SLP during winter (Table 6), plus an increase in the speed and propagation of low SLP anomalies in time-longitude diagrams (not shown), which look similar to the variability seen in Figure 2 for low-cloud cover. Additionally, the power spectrum for SLP (not shown), as well as those of other dynamic variables, has an order of magnitude less power at seasonal time scales and more power at synoptic time scales (defined roughly as 3-10 days) than the static stability spectra. The shape of the power spectra for cloud properties falls somewhere in between the static stability and the SLP spectra.

Similar to what we see in the subtropics, this type of time-longitude variability has been observed for cloud properties in the tropics. Chang (1970), noting the westward propagation of clouds across the tropical Pacific ocean during July and August, hypothesized that these patterns could be due either to the passage of wave disturbances or the advection of cloud clusters by the mean flow. He turned to several analyses of rawinsonde SLP data to confirm that observed cloud variations were the result of easterly waves with periods of 3-5 days and estimated wavelengths of thousands of kilometers. Cho and Ogura (1974) connected the increasing high-level cloud coverage associated with the troughs of the tropical easterly waves to increases in low-level convergence.

This type of disturbance is observed in the variability of cloud properties in the Canarian region during summer. Summertime disturbances could be the result of the easterly waves originating on the African continent, with wavelengths of approximately 2500km and periods of about 3-4 days (e.g. Burpee 1972; Reed et al. 1977). These waves have been studied extensively to determine their link to hurricane development and to chart their progress across the tropical Atlantic. They appear in the Canarian region as increases in surface observed upper-

level cloudiness and negative SLP anomalies (e.g. Carlson 1969).

In the following sections, we examine the variability of cloud and meteorology together by compositing. Compositing allows us to study relationships between variables without making assumptions about the shapes of the frequency distributions. In the following sections we discuss selected variables in depth and summarize the remaining results.

1. NH during NDJFM

a. Cloud properties composited by dynamic anomalies

The results for the following section are summarized in Table 7. Following the examples of Tselioudis et al. (2000) and Lau and Crane (1995, 1997), we examine anomalies in SLP and find that days of negative SLP anomaly (lower pressure) are associated more often with higher-altitude clouds and lower-altitude, thinner (smaller TAU) clouds in both regions (the Californian region is shown in Figure 8). Unlike the studies mentioned above, these data are spatially averaged so the dispersion seen these figures is due entirely to temporal variability.

We extend this analysis to include other variables. Figure 9 shows that thicker and thinner clouds at all altitudes are better separated by anomalies in the magnitude of Δ_vSLP across the region, a negative Δ_vSLP anomaly being associated with thicker clouds. A negative Δ_vSLP value occurs when the SLP on the poleward side of the box is larger than the equatorward side. Therefore, a negative Δ_vSLP anomaly occurs either when this gradient is large and negative or when the monthly mean meridional pressure gradient is larger and more positive than the daily value. Thicker clouds also tend to be associated more often with negative U_{1000} anomalies (weaker zonal winds) during this season.

Anomalies in ω_{700}, U_{shear}, V_{1000}, and $\Delta_v T_{1000}$ divide subtropical cloud properties into smaller and larger CTP regimes; but the division is most clear for anomalies in ω_{700} (Fig-

ure 10) and U_{shear} (Figure 11). Since ω_{700} is positive for descent and seasonally averaged ω_{700} is always positive, positive ω_{700} anomalies represent times of increased descent. In this figure, increased descent is associated with larger CTPs (or lower-altitude cloud tops). However, anomalies in ω_{700} have no apparent relationship to TAU variations. Smaller CTP clouds are associated with negative V_{1000} anomalies (stronger equatorward wind speeds) and negative $\Delta_v T_{1000}$ anomalies (warmer advection if the meridional wind direction is poleward, or less strong cold advection if its equatorward).

Larger anomalies of U_{shear} are due primarily to increases in U_{500}. Since increasing vertical shear is related to departures from barotropic stratification through the thermal wind equation (Salby 1996), it is not surprising that increasing shear between these levels is associated with more frequently occurring smaller CTP (upper-level) clouds.

In order to separate clouds into CTP and TAU categories at the same time, the cloud data are sorted by the Δ_vSLP and ω_{700} criteria together. Since correlations between seasonal anomalies of Δ_vSLP and ω_{700} are poor in the NH subtropics during this season (r values of -0.1), we can sort the data using both criterion without redundancy. In Figure 12, higher-altitude, thicker clouds are most often associated with negative anomalies in Δ_vSLP and ω_{700}. These tend to be times where Δ_vSLP is large and negative and upward ω_{700} (ascent). Lower-altitude, thinner clouds occur on days that have positive (smaller) values of Δ_vSLP and downward ω_{700}. The distribution using both criteria more closely resembles the ω_{700} distribution, with the Δ_vSLP criterion causing slight shifts in the TAU categories.

These results are consistent with previous work. Some modeling studies have found a similar association between larger downward vertical velocities and larger CTPs (or thinner

boundary layers), but until now no relationship to physical cloud thickness or TAU has been noted (e.g. Schubert et al. 1979; Hack et al. 1989; Philander et al. 1996). Data analyses of storms over the NH midlatitude oceans have concluded that local ascent and descent in mid-latitude synoptic scale disturbances are associated respectively with smaller and larger CTPs (Lau and Crane 1995; 1997), and larger and smaller longwave cloud radiative forcing (Weaver and Ramanathan 1997).

b. Cloud properties composited by temperature anomalies

Compositing cloud variables by anomalies in temperature emphasizes different relationships than compositing by actual temperature. This study differs from Tselioudis et al. (1992) and Tselioudis and Rossow (1994) because they examined the actual temperature dependence of TAU and how its sign changes with season and latitude while neglecting dynamically-induced variations. In our case, looking at dependence of TAU on seasonal anomalies in temperature is intended to isolate the contribution of synoptic changes in temperature to changes in TAU, while neglecting the actual temperature dependence of TAU. This study is also limited to the eastern ocean, rather than including all longitudes over the ocean.

Static stability anomalies (not shown) do not divide cloud properties into well-defined regimes in either region during this season. When taken separately, colder θ_{740} and surface temperature anomalies (not shown) both appear to be weakly associated with thicker clouds. If a colder temperature anomaly is equal to a colder actual temperature, this is consistent with Tselioudis et al. (1992) and Tselioudis and Rossow (1994). If we composite the cloud data by actual stability and temperature values rather than seasonal anomalies, we find larger CTP and thicker clouds to be weakly associated with larger values of stability and colder θ_{740} and sur-

face temperatures. The relationships between composited cloud properties and actual temperatures are stronger than in the seasonal anomaly case. Therefore, temperature may not be a good diagnostic for examining variability of cloud properties due to synoptic wave passage.

In an alternate experiment, we composited cloud properties using stability and temperature anomalies from ERA. In this case, positive anomalies in static stability are strongly associated with thicker, larger CTP clouds. ERA temperature anomalies associate thicker, larger CTP clouds with both warmer θ_{700} temperatures and colder θ_{1000} temperatures; therefore both variables appear to be contributing to the relationship with ERA static stability. When we repeat the analysis using actual temperature values instead of anomalies, we find that ERA does show thicker clouds associated with larger values of stability and colder θ_{1000} temperatures, but we also find them associated with warmer θ_{700} temperatures, in disagreement with our results with TOVS.

The relationships between stability and temperature anomalies and cloud properties are clearly weaker for TOVS anomalies than ERA anomalies, and in some cases, even the sign of the relationships is different between the datasets. Although ERA does incorporate TOVS data into its reanalysis, it uses TOVS radiances rather than the operational data products. As discussed in the data section, a recent study (Stubenrach et al. 1999) shows that monthly TOVS temperatures over tropical and subtropical ocean regions tend to be colder at the surface and warmer at 740mb compared to 3I sounding data. Since this is true for both the January and July data, this probably causes TOVS to systematically overestimate the mean static stability in both seasons. However, whether this would affect the daily variability is less certain. Although TOVS radiances are available twice per day, the TOVS operational product uses data from only one time per day (Stubenrach et al. 1999). The time of day and the source

(satellite) for this profile can vary within a month. On the other hand, the effect of the ERA model assimilation process on this particular feature of the assimilation process is unknown.

Given what we know about both datasets, we cannot come to a definitive conclusion about the relationships seen here between static stability, temperature anomalies and cloud properties. Addressing these discrepancies would involve cross-correlations between the temperature variables within each dataset and across the two datasets plus an investigation into the causes of daily temperature variability in both datasets. While this subject is worth further investigation, we will not attempt to do so here.

2. MJJAS in all regions and NDJFM in the SH

As mentioned earlier, previous studies of intraseasonal data found larger low-cloud fractions associated with increases in static stability, cold advection, subsidence and strength of the subtropical high. In this section, we test these relationships using our data and extend the results to include changes in the CTP-TAU frequency distribution. Since the intraseasonal variability of cloud properties during this season is smaller in amplitude than either the seasonal cycle or the synoptic NH winter variability, particularly in CTP, we initially increased the number of CTP and TAU categories as described in the data section of this paper. However, none of the variables tested produced a clear separation in cloud regimes. Since we know that the time scales of variability during this season are longer than weeks to months, subtracting monthly means from the data may obscure the information we are interested in. In this case, we obtained better separation between cloud regimes by compositing data by actual meteorological values, rather than anomalies. This method is also described in the data section of the paper.

a. Cloud properties composited by dynamic variables

We tested several other variables to verify relationships observed in surface data studies (see Table 8). Larger SLP values (stronger subtropical highs) are found more often with thicker TAU clouds in all regions and smaller CTPs (higher-altitude cloud tops) in the NH (Figure 13). This result was unexpected given that we tend to associate stronger subtropical highs with increasing subsidence and lower-altitude cloud tops. Larger, positive values of ω_{700} (larger subsidence) are weakly associated with thinner TAU and decreasing low and total cloud fractions. Larger 1000mb wind speeds are associated with thicker, larger CTP clouds and increasing cloud coverage in all regions except for the Peruvian. Larger, negative values of V_{1000} (in the NH, these are larger equatorward meridional wind speeds) are associated with thicker clouds in the Californian region only. In contrast, larger positive $\Delta_v T_{1000}$ (larger meridional temperature difference) are associated with thicker clouds only in the SH regions. U_{shear} tends to be associated with smaller CTP values in all regions, but has a mixed relationship to cloud fraction and TAU.

Clearly, these relationships are not always consistent for all regions. This could be due to a variety of reasons, one being the problem of trying to resolve small amplitude variability in the meteorology fields. Norris and Klein (2000) have better success compositing ω_{700} anomalies by surface-observed cloud-types. If we assume for a moment that changes in ISCCP cloud properties are easier to resolve than changes in dynamic variables, we can follow their example and composite dynamic variables by daily average values of TAU and CTP.

In this case, when we composite by CTP, lower-altitude clouds are associated consistently with larger values of SLP for all regions. This result also holds true for the SH regions during local winter and is consistent with our earlier result. However, there appears to be no consistent relationship between CTP and ω_{700}. If we composite by TAU, we find thicker

clouds associated with high SLPs in the Californian region and a weak relationship with upward vertical velocities in the remaining three regions. Performing the analysis in this way does not appear to provide additional information, possibly because amplitudes of cloud variability are also smaller during this season, particularly for CTP. In general, the same relationships are obtained whether one composites the cloud properties by dynamics or the dynamics by cloud properties.

b. Cloud properties composited by temperature variables

Of the variables tested in Klein (1997), static stability (either using TOVS/ISCCP data or ERA) separate cloud properties most clearly into particular types (Figure 14). Consistent with Tselioudis et al. (1992), warmer upper atmosphere temperatures (θ_{740} from TOVS or θ_{700} from ERA) are associated with thicker, lower-altitude clouds during this season in all regions except the Namibian, where these clouds are found with colder temperatures. Colder surface temperatures are associated with thicker clouds for all regions.

V. Discussion

Sorting the NH NDJFM cloud data by seasonal anomalies in ERA meteorology shows that large changes in cloud properties are better related to changes in the large-scale circulation than to changes in boundary layer parameters in both seasons. The combined criteria in Figure 12 show that thicker, higher-altitude cloud tops tend to be associated with larger meridional SLP gradients and more negative (upward or less strong downward) ω_{700} anomalies. This is generally the warm sector of the synoptic storm, after the warm front passage and ahead of the cold front.

Despite the small amplitude variability during MJJAS, we repeat our composite analysis for this season using actual variable values rather than anomalies. Some relationships are

found to be consistent with previous studies, others are not. The relationships that are found to be consistent do not always seem to be true for all subtropical regions.

Two types of intraseasonal low-cloud variability seem to dominate the subtropics - the storm driven NH wintertime variability and the longer time period NH summer and SH variability. In the following sections, we discuss each type separately.

A. NH in winter

What does the passage of a synoptic wave do to the vertical structure of the subtropical boundary layer and thus to low clouds? Under undisturbed conditions, the vertical structure consists of subcloud and cloudy layers capped vertically by a temperature inversion (sample soundings for the subtropical oceans are shown in Schubert et al. 1979, Nicholls 1984; Albrecht et al. 1995b; Norris 1998). Since these layers are seldom well-mixed, it is common to find profiles of q decreasing with height, and θ and θ_e increasing with height below the inversion.

As the synoptic wave passes, large-scale convergence and ascent occurs just preceding the low SLP anomaly (Lau and Crane 1995). As the air in the boundary layer is synoptically lifted, the entire subcloud layer cools at the adiabatic lapse rate. However, if q decreases with height, lower layers may reach saturation before upper layers and subsequently cool more slowly. This can destabilize the subcloud layer and cause vertical mixing. Non-uniform cooling can also destabilize the temperature inversion. Sarachik (1979) points out that large-scale lifting could cause the dry air above the inversion air to cool more rapidly than the cloudy air just below it, resulting in rapid instability and vertical mixing which could temporarily wipe out the temperature inversion. This is consistent with data from ships N and P, which show that wintertime soundings associated with anomalously low SLP more often have higher-altitude inversion heights or no inversion compared to soundings associated with positive SLP

anomalies (Figure 15 and Table 9).

We study the effect of synoptic wave passage on the subtropics by asking two slightly different questions. How long do higher-altitude clouds linger in the subtropical regions? Once the synoptic wave passes, how long before the vertical structure of the subtropical boundary layer returns to a "normal" state? To answer the first question, we chose a threshold of CTP=560mb (the mid-point of the middle cloud category) and ask the question, once the daily average CTP goes below this critical value, how long does it remain there? In most cases, daily CTP stays below this value for 2-3 days, but occasionally smaller CTPs persist for as long as 8 days. The inversion also reappears in 2-6 days, with few exceptions. Both of these time scales are consistent with synoptic wave passage.

If the storm-track did not intrude into the subtropical NH regions in winter, would low-cloud intraseasonal variability look similar to the summer season? We cannot answer this question since the synoptic storms and their effects cannot be completely removed from the data. However, answering a related question may give us new insight. Given that most of the MJJAS intraseasonal variability exists under subsidence conditions, can the relationships found during MJJAS between clouds and meteorology be seen in the NDJFM during the increased subsidence phase of the wave?

We investigate this using a subset of the winter data, keeping only data where both the actual value of ω_{700} and the ω_{700} seasonal anomaly are positive. Then, using the MJJAS median anomaly values, this subset is separated into positive and negative composites. Subtracting these composites produced the same relationships seen in Table 8, where thicker clouds and larger low-cloud fraction are associated with positive anomalies in static stability and SLP. This result hints that if synoptic variability did not disturb the region, intraseasonal

variability during winter would probably look similar to the summer case. In addition, Figure 16a shows that when descent in the Californian region is anomalously large (downward), the spatial SLP anomaly pattern is largely zonal with high pressure dominating the subtropics. In the case where the ω_{700} anomaly is negative (Figure 16b), the SLP anomaly pattern shows the synoptic wave structure with anomalous descent over the subtropics.

The interaction of the of synoptic variations in meteorology, cloud properties and underlying SSTs in the subtropics adds a non-linear dimension to the problem of air-sea interaction. The time scale of synoptic wave effects on cloud properties is on the order of days and the spatial scale is thousand of kilometers. Although both the atmosphere and the ocean surface experience changes in radiation and temperature on these scales, the oceanic response to these changes occurs more slowly than the atmospheric.

B. Californian in summer and SH in both seasons

During this season the influence of intraseasonal variability on the boundary layer is much weaker (Figure 17), but the variability of the inversion height with anomalies in SLP can still be seen (Figure 18). As summarized by Miller (1997), the temperature and moisture structure of the atmosphere above the subtropical boundary layer depends to a great extent on the large-scale tropical circulation. Therefore, the variability of clouds and meteorology are largely determined as a balance between tropically-driven upper atmosphere conditions and local subtropical boundary layer processes. As mentioned earlier, several studies test the links between tropical and subtropical variability using box models (Sarachik 1978; BR89; Miller 1997; Clement and Seager 1999; Larson et al. 1999). For example, BR89 couple a tropical convective region to a subsiding region by assuming that the temperature profile in the convective region is fixed to a moist adiabat and that upper-level temperature gradients above

both regions are small. This makes temperature and moisture profiles above the trade inversion determined by profiles in the tropics. Thermodynamic properties of air in the subsiding region are assumed to lie on a mixing line joining the conserved total water and θ_e just above the inversion to values near the ocean surface.

BR89 test the dependence of their results on the equilibrium time scale of the convective boundary layer by using different closure assumptions. To do this, they assume that some of the time scales in question are separable; some processes occur so rapidly compared to others, that the slow ones are essentially fixed. These assumptions are important because BR89 find that relationships between meteorology and cloud properties can vary in magnitude, and even in sign, depending on the time scale and type of coupling that is assumed. In the case that is probably closest to our intraseasonal time scale, they assume that the troposphere is in energy balance, with an associated time scale of approximately ten days. For this experiment, surface fluxes of latent and sensible heat (LH and SH) in the subsidence region are balanced by the radiative flux divergence between the troposphere and the surface. In this section, we compare the results of these experiments to the relationships found in our data in the hope of linking observed changes in the large-scale circulation and low-level clouds to a modulation of boundary layer processes by the large-scale circulation.

In Table 8, the sign of the relationship between surface temperature and TAU is partially consistent with surface observations from Norris (1998 - Figure 3), who finds Cu type clouds at ship N associated with warmer values of θ_e (and presumably SST, although this is not shown explicitly). However, Norris also finds that higher-altitude inversion heights are associated with Cu clouds rather than Sc, which appears to be inconsistent with our results. But since the observed difference in pressure at the inversion base between the two compos-

ite soundings in his figure is about 50mb and our bin widths are approximately 60mb, our results may not be sensitive to this change. In the model of BR89, increasing SST increases low-level θ_e and decreases CTP (low-cloud fraction is held fixed in their model). This occurs because, for a fixed surface wind speed, increasing SST increases the SH and LH fluxes (where these fluxes are determined by bulk aerodynamic formulas). To maintain tropospheric energy balance, this extra energy can be compensated by a decrease in the outgoing longwave flux by clouds represented by a decrease in the cloud-top temperature. This can occur either by decreasing the CTP (for a fixed lapse rate) or by increasing the lapse rate (for fixed CTP). The BR89 model does a combination of these things, resulting in equilibrium CTPs that decrease less rapidly with increasing SST compared to runs where the model can only respond by changing CTP (see their Figure 13).

Similarly, BR89 find that increasing the surface wind speed increases low-level θ_e and decreases CTP. In this case, although LH increases, SH decreases because although the wind speed is increasing, the temperature difference between the SST and the overlying air decreases. However, since the LH flux is two orders of magnitude larger than the SH flux, its increase must again be balanced by a decrease in the cloud-top temperature.

BR89 show that in the coupled troposphere case, subsidence is not an external parameter, but decreases with increasing SST and wind speed. Therefore, the effect of decreasing subsidence on cloud parameters should be the same as discussed in the previous two cases. However, our data show only a slight increase in low-cloud fraction with decreasing ω_{700} (less subsidence) in all regions and no apparent relationship to TAU or CTP.

Under this same argument, BR89 speculate that increasing SLP should be associated with increasing subsidence and thinner, larger CTP clouds. However, we find that larger SLPs

are more often associated with thicker, smaller CTP clouds. This is more consistent with Klein (1997), who interprets an increase in SLP as an increase in cold advection. However, changes in surface air properties through advection are not addressed by BR89.

Increasing moisture above the boundary layer causes a sharp increase in CTP (approximately 50mb with every g/kg of total water). This is a steeper response than the uncoupled case because the addition of total water decreases the radiative cooling and increases the subsidence at cloud-top. We tested this possibility using S_{700} from ERA and PW_{up} from TOVS, but found results which are mixed in sign and inconsistent between regions (therefore, these results are not included in Table 8.

Although some of the relationships seen in the data between cloud properties and meteorology can be better understood though the model of BR89, there are enough disagreements to imply that this may not be an adequate model to explain the MJJAS variability in boundary layer cloud properties in all regions. In particular, the model does not account for changes in the advection of temperature and moisture. Unfortunately, adding more complexity to a model of this kind may make it impossible to interpret the results. Additionally, inconsistencies could be the result of problems with ISCCP data or ERA meteorology. Understanding the reasons for these disagreements may require additional long term measurements in the subtropical regions, particularly in the SH, where little meteorological data is assimilated into ERA.

VI. Conclusions

We have explored the role of the general circulation in the large-scale variability of subtropical marine low-level cloud properties. Longer time scale processes change the basic state of the subtropics and the more rapid processes at work within it. These interactions on differ-

ent time scales make the variability non-local; this may account for the limited success of attempts to describe the system using only local, linear or single variable analyses.

The longer period seasonal cycle plays a modulating role on daily to monthly variability. With the exception of the Canarian region, CTP-TAU frequency distributions indicate that these subtropical regions are more frequently populated by lower-altitude clouds with a wide range of thicknesses during the NH summer season. This pattern is altered during the winter season in the Californian region and during both seasons in the Canarian by large-scale synoptic variations in both cloud properties and meteorology. We have examined changes in cloud properties and meteorology as they occur together, and have speculated that changes in cloud properties could be the result of changes in meteorology, although there is reason to believe that the reverse can also be true (e.g. Clark 1993). These differences highlight the difficulty of treating the seasonal cycle as decoupled from other time scales of variability. Our inability to consistently explain the seasonal variability in all four subtropical regions may be due in part to the fact that part of the apparent cycle (e.g. the minimum values of low-cloud fraction during the NDJFM season) occurs for different reasons in different locations.

Our attempt to explain the intraseasonal variability in the NH summertime and SH as a result of interactions with changing tropical convection had limited success. The single box model of BR89 predicts that clouds in subsiding regions will increase in TAU and decrease in CTP with increasing SST, decreasing subsidence, increasing surface wind speed or increasing the specific humidity above the inversion. Comparisons with our data show mixed agreement with these model predictions and the results of surface-based studies, particularly when data from both hemispheres are considered. The large number of inconsistent results between our data, surface-observed studies and the BR89 model illustrates the need for additional long-

term observations of cloud and meteorology. To add to this analysis, these data need to include simultaneous cloud property and meteorological data in both hemispheres, for both seasons, and consider sufficient resolution in cloud CTP and TAU.

The model of BR89 cannot be used to test the larger amplitude variations induced by synoptic waves during the NH winter season since assumptions of continuous subsidence above the boundary layer and an equilibrium balance between the boundary layer and upper atmospheric parameters are violated in this situation. A different type of model needs to be used to study the effects of frontal passage on boundary layer processes, vertical structure and cloud properties. One possibility is to use a single-column model and simulate the passage of a front using a time-varying ω_{700}, and/or a temperature gradient at the surface. Simulating the NH winter case study might be a more useful way to diagnose whether GCM low-cloud model deficiencies are due to problems with the dynamics or with the cloud parameterizations since the intraseasonal variability in clouds properties and meteorology are much larger in amplitude.

Acknowledgments. The authors would like to thank Brian Cairns, Ron Miller and George Tselioudis for insightful comments during the progress of this work. Ralph Karow and Fabio Diniz also provided invaluable computer support. MAR is supported by a NASA-GISS cooperative agreement with the Department of Applied Physics at Columbia University, grant NCCS-485.

Figure Captions

Figure 1. Temporal spectrum of daily average ISCCP total cloud TAU on the 10x10° spatial scale for nine years (1984-92) for the four regions of Table 1. A line representing a power law with exponent -1 is shown for reference.

Figure 2. Time-longitude diagrams of daily average ISCCP low cloud fraction at 25-30°N for January - December 1990 (results are similar for other years). The Californian region is located approximately between 230-240° longitude on this diagram.

Figure 3. Persistence (in days) of low cloud fraction events larger than 70% during MJJAS and NDJFM (1984-92). Distributions are normalized by the total number of events for that season.

Figure 4. Frequency distributions of daily average ISCCP low-cloud fraction (1984-92) on 2.5x2.5° and 20x20° spatial scales for MJJAS and NDJFM.

Figure 5. Same as Figure 4, but for ISCCP total cloud TAU.

Figure 6. 2D frequency distributions of daily average ISCCP total cloud TAU and CTP (1984-92) for the 10x10° domain. Solid lines are MJJAS and dotted lines are NDJFM.

Figure 7. (a) Time series of the monthly mean spatial standard deviation of ISCCP (1984-92) total cloud CTP for the Californian region and selected tropical Pacific ocean domains from Table 5. (b) Correlation when the Californian region is lagged (in months) behind the tropical regions. (c) Correlation when the Peruvian region is lagged behind the tropical regions.

Figure 8. 2D frequency distributions of daily average ISCCP total cloud TAU and CTP sorted by ERA seasonal SLP anomalies, CAL NDJFM (1984-90). Mean low and

total cloud fractions associated with each composite are printed in the upper left hand corner.

Figure 9. Same as Figure 10d, but for anomalies in ERA Δ_vSLP.

Figure 10. Same as Figure 10d, but for anomalies in ERA ω_{700}.

Figure 11. Same as Figure 10d, but for anomalies in ERA vertical shear of the zonal wind (U_{500}-U_{1000})

Figure 12. Sorting ISCCP total cloud TAU and CTP by ERA ω_{700} and Δ_vSLP anomalies together during NDJFM (1984-90).

Figure 13. Cloud properties associated with smaller - larger ERA SLP values for MJJAS in the four subtropical regions.

Figure 14. Cloud properties associated with smaller - larger static stability values for MJJAS in the four subtropical regions.

Figure 15. Dependence of pressure at the base of the temperature inversion on SLP anomaly during NDJFM at ships N and P. The total number of soundings used in the frequency distribution is printed on the figure.

Figure 16. Spatial pattern of composite SLP anomaly for NDJFM (1989-90) over the northern Pacific ocean when ω_{700} anomalies in the 10x10° Californian region are positive and negative.

Figure 17. Spatial pattern of composite SLP anomaly for MJJAS (1989-90) over the northern Pacific ocean when SLP anomalies in the 10x10° Californian region are positive and negative.

Figure 18. Dependence of pressure at the base of the temperature inversion on SLP anomaly during MJJAS at ships N and P. The total number of soundings used in the fre-

quency distribution is printed on the figure.

REGION	LATITUDE	LONGITUDE
CAL	20-30 N	120-130 W
PER	10-20 S	80-90 W
CAN	15-25 N	20-30 W
NAM	10-20 S	0-10 E

Table 1.

Cloud Fraction

REGION	IR			VIS/IR							
MJJAS	**Low**	**Mid**	**Hi**	**Low**	**Ran**	**Mid**	**Hi**	**St**	**Sc**	**Cu**	**Total**
CAL	58.8	9.9	2.9	65.4	76.7	10.5	4.5	7.8	45.0	12.7	81.8
PER	66.2	6.4	0.2	65.9	73.5	9.0	1.7	2.3	46.4	17.2	81.6
CAN	37.6	7.5	3.1	43.1	50.6	8.0	7.6	1.1	21.0	20.9	60.8
NAM	62.9	4.9	0.2	66.2	73.1	7.5	2.4	4.2	49.1	13.0	78.2
NDJFM											
CAL	48.2	14.5	11.0	45.7	66.3	14.6	16.6	1.9	27.1	16.8	79.6
PER	52.5	8.7	0.8	48.0	57.1	11.7	3.6	3.8	31.0	13.2	66.5
CAN	36.2	9.3	8.2	34.2	46.1	10.0	16.2	0.8	12.3	21.1	64.9
NAM	57.6	3.9	0.4	57.8	64.1	6.2	4.1	3.8	43.3	10.8	70.4
MJJAS-NDJFM											
CAL	10.6	-4.6	-8.6	19.7	10.4	-4.1	-12.1	5.9	17.9	-4.1	2.2
PER	13.7	-2.3	-0.6	17.9	16.4	-2.7	-1.9	-1.5	15.4	4.0	15.1
CAN	1.4	-1.8	-5.1	8.9	4.5	-2.0	-8.6	0.3	8.7	-21.1	-4.1
NAM	5.3	1.0	-0.2	8.4	9.0	1.3	-1.7	0.4	5.9	-0.6	7.8

Cloud Optical Thickness and Location of Cloud Top

REGION	Low Cloud							Total Cloud				
MJJAS	**TAU**	**LWP**	**St TAU**	**Sc TAU**	**Cu TAU**	**CTT**	**CTH**	**TAU**	**LWP**	**CTT**	**CTP**	**CTH**
CAL	8.9	86.1	29.6	8.0	2.3	285.8	1277	8.1	70.2	281.6	755	1923
PER	4.9	48.7	30.3	7.5	2.5	284.7	1308	10.6	44.5	281.6	750	1784
CAN	2.4	30.0	39.3	6.3	2.0	289.8	1092	3.6	32.0	281.1	735	2431
NAM	6.8	63.7	27.2	8.3	2.2	285.8	1200	8.4	53.0	282.2	765	1754
NDJFM												
CAL	3.9	45.1	34.7	8.0	2.3	282.2	1615	5.6	47.5	272.1	675	3169
PER	5.8	63.3	30.3	7.3	2.2	285.2	1585	6.6	43.1	280.5	715	2308
CAN	1.5	24.2	60.4	6.2	1.7	286.8	1415	3.4	29.1	273.8	685	3415
NAM	7.1	65.3	27.8	8.3	2.2	288.3	1107	7.9	51.0	282.7	750	1969
MJJAS-NDJFM												
CAL	5.0	41.0	-5.1	1.2	0.3	3.6	-339	2.5	22.7	9.5	80	-1245
PER	-0.9	-14.6	0.0	0.2	0.0	-0.5	-277	4.0	1.4	1.1	35	-523
CAN	0.9	5.8	-21.1	0.1	0.3	3.0	-323	0.2	2.9	7.3	50	-985
NAM	-0.3	-1.6	-0.6	0.0	0.0	-2.5	92	1.5	2.0	-0.5	15	-215

Tables 2a and 2b.

REGION	> 70%		>50%	
	MJJAS	NDJFM	MJJAS	NDJFM
CAL	95	56	82	92
PER	75	36	109	85
CAN	13	16	60	54
NAM	78	67	103	94

Table 3.

REGION	r^2	slope	y-intercept
low cloud			
CAL	0.74	5.22	-13.04
PER	0.52	3.71	2.26
CAN	0.56	3.48	-1.46
NAM	0.72	4.99	-11.64
ALL	0.73	4.97	-13.79
random overlap cloud			
CAL	0.61	2.89	33.11
PER	0.59	4.22	3.46
CAN	0.36	2.27	22.27
NAM	0.70	5.14	-7.02
ALL	0.59	4.17	7.16
maximum overlap cloud			
CAL	0.20	1.16	62.84
PER	0.57	3.72	15.46
CAN	(0.01)	0.26	56.78
NAM	0.74	5.27	4.54
ALL	0.38	2.65	34.56

Table 4.

REGION	LATITUDE	LONGITUDE
PAC1	5S-15 N	150-180 E
PAC2	5S-15 N	180-150 W
PAC3	5S-15 N	150-120 W
PAC4	5S-15 N	120-90 W

Table 5.

ERA Sea Level Pressure

REGION	MJJAS				NDJFM			
	MEAN	STD	ANOM RANGE		MEAN	STD	ANOM RANGE	
CAL	1018.4	2.3	-7.8	9.0	1020.5	3.7	-17.3	8.1
PER	1018.4	2.3	-8.4	6.5	1016.2	1.9	-5.5	5.3
CAN	1018.3	1.7	-5.7	5.1	1018.9	2.7	-9.8	6.4
NAM	1021.9	2.4	-7.5	6.0	1016.1	2.0	-5.0	5.2

Table 6.

NDJFM	change in cloud properties			
Variable	LCF	TCF	TAU	CTP
SLP	increase	increase	thicker	larger
Δ_vSLP, U_{1000}	decrease	decrease	thinner	none
ω_{700}	increase	decrease	none	larger
Vertical Shear (U_{500}-U_{1000})	decrease	increase	none	smaller
V_{1000}	decrease	none	none	smaller
$\Delta_v T_{1000}$	none	increase	none	smaller
$\Delta_u T_{1000}$	none	decrease	none	larger
T_{1000}, Clear Sky Temp	decrease	decrease	thinner	smaller
T_{700}	increase	none	thicker	larger
STAB	none	none	none	none
ERA STAB	increase	none	thicker	larger

Table 7.

MJJAS	change in cloud properties				regions affected
Variable	**LCF**	**TCF**	**TAU**	**CTP**	
SLP	increase(SH)	increase(SH)	thicker	smaller (NH)	ALL
Δ_vSLP	decrease	decrease	thinner	none	CAN and NAM
Δ_uSLP	decrease	none	thinner (except NAM)	amaller	ALL
ω_{700}	decrease	none	none	smaller	ALL(weak)
U_{1000}	decrease	decrease	thinner(NH)	larger	ALL
$\Delta_u T_{1000}$	decrease	decrease	thinner	none	ALL
V_{1000}	decrease (except NAM)	decrease (except NAM)	thinner(CAL)	none	ALL
$\Delta_v T_{1000}$	decrease(SH)	decrease(SH)	thinner	smaller(CAL)	ALL
SPEED	increase (except PER)	increase (except PER)	thicker(NH)	smaller	ALL
Vertical Shear (U_{500}-U_{1000})	decrease	none	thinner	smaller	ALL except NAM
STAB	increase	increase	thicker	none	ALL
Clear Sky Temp	decrease(SH)	decrease	thinner	none	ALL
TOVS θ_{740}	increase	increase	thicker	larger	ALL except NAM
ERA STAB	increase	increase	thicker	none	ALL
ERA θ_{1000}	decrease(SH)	decrease	thinner	none	ALL
ERA θ_{700}	increase	none	thicker	none	All except NAM

Table 8.

REGION	POS SLP ANOM			NEG SLP ANOM		
	MODE	MEAN	STD	MODE	MEAN	STD
NDJFM						
CAL	279 (742)	276 (727)	7 (97)	285 (895)	271 (675)	11 (127)
SHIPN	292 (825)	294 (828)	3 (43)	298 (825)	298 (804)	3 (53)
SHIPP	282 (875)	283 (824)	4 (88)	287 (725)	286 (740)	12 (108)
MJJAS						
CAL	288 (755)	280 (736)	6 (75)	286 (773)	284 (781)	4 (62)
SHIPN	296 (875)	296 (852)	3 (41)	300 (825)	300 (824)	3 (46)
SHIPP	289 (875)	288 (882)	4 (62)	293 (775)	290(805)	3 (63)

Table 9.

Table Captions

Table 1: Boundaries of the 10x10° regions. Other sizes are concentric around the given boundaries. The 2.5x2.5° region is the box most equatorward and westward within the 5x5° region. The Canarian region is shifted 5° west from KH93 to avoid coastal influences.

Table 2: (a) ISCCP D2 (1984-92) seasonal averages and differences for cloud fraction (%). Cloud fraction information is separated into types as defined by ISCCP. These types include low-level (Low), low-level corrected using a random overlap assumption (Ran), mid-level (Mid), high-level (Hi) and total cloud. Cloud fractions associated with St, Sc and Cu optical thicknesses are also included. (b) ISCCP D2 (1984-92) seasonal averages and differences for TAU, LWP (g/m^2), CTP (mb), CTH (meters) and CTT (°K).

Table 3: Number of times low-cloud fraction surpasses the given threshold cloud fraction (10x10° regions) by season (1984-92).

Table 4: Correlation coefficients, slopes and y-intercepts for a linear fit to seasonal anomalies (annual mean removed) in ISCCP low-cloud fraction and static stability. Results are also shown when low-cloud fraction is corrected using assumptions of random and maximum overlap. Correlations not significant at the 99% level are in parentheses.

Table 5: Boundaries of the tropical Pacific regions.

Table 6: Mean, standard deviation and range for ERA SLP by season for the regions of Table 1.

Table 7: Changes in composite cloud properties associated with positive anomalies in meteorology for the Californian and Canarian regions only during NDJFM. Increases or

decreases in cloud fraction are included if the amount exceeds 5%.

Table 8: Changes in composite cloud properties associated with increases in meteorological variables for all regions during MJJAS. Increases or decreases in cloud fraction are included if the amount exceeds 5%.

Table 9: Mode, mean and standard deviation of composite temperatures and pressures (in parentheses) for SLP anomalies during MJJAS and NDJFM. CAL pressures (mb) and temperatures (degrees K) are those of the ISCCP cloud top; SHIP pressures and temperatures are those associated with the base of the temperature inversion.

Bibliography

Albrecht, B. A., C. S. Bretherton, D. Johnson, W. H. Schubert, and A. S. Frisch, 1995a: The Atlantic Stratocumulus Transition Experiment - ASTEX. *Bull. Amer. Meteor. Soc.,* **70**, 889-904.

Albrecht, B. A., M. P. Jensen, and W. J. Syrett, 1995b: Marine boundary layer structure and fractional cloudiness. *J. Geophys. Res.*, **100**, 14,209-14,222.

Barker, H. W., 1996: A parameterization for computing grid-averaged solar fluxes for inhomogeneous marine boundary layer clouds. Part I: Methodology and homogeneous biases. *J. Atmos. Sci.*, **53**, 2289-2303.

Bechtold, P., S. K. Krueger, W. S. Lewellen, E. van Meijgaard, C.-H. Moeng, D. A. Randall, A. van Ulden, and S. Wang, 1996: Modeling a stratocumulus-topped PBL: Intercomparison among different one-dimensional codes and with large eddy simulation. *Bull. Amer. Meteor. Soc.*, **77**, 2033-2042.

Bergman, J., and M. Salby, 1996: Diurnal variations of cloud cover and their relationship to climatological conditions. *J. Climate*, **9**, 2802-2820.

Betts, A. K., 1990: Diurnal variation of California coastal stratocumulus from two days of boundary layer soundings. *Tellus*, **42A**, 302-304.

Betts, A. K., and W. Ridgway, 1989: Climatic equilibrium of the atmospheric convective boundary layer over a tropical ocean. *J. Atmos. Sci.*, **46**, 2621-2641.

Blaskovic, M., R. Davies, and J. B. Snider, 1991: Diurnal variation of marine stratocumulus over San Nicholas Island during July. *Mon. Wea. Rev.*, **119**, 1469-1478.

Bolton, D., 1980: The computation of equivalent potential temperature. *Mon. Wea. Rev.*, **108**, 1046-1053.

Bretherton, C. S., E. Klinker, A. K. Betts, and J. A. Coakley Jr., 1995: Comparison of ceilometer, satellite, and synoptic measurements of boundary-layer cloudiness and the ECMWF diagnostic cloud parameterization scheme during ASTEX. *J. Atmos. Sci.*, **52**, 2736-2751.

Burpee, R. W., 1972: The origin and structure of easterly waves in the lower troposphere of North Africa. *J. Atmos. Sci.*, **29**, 77-90.

Cairns, B., 1995: Diurnal variations of cloud from ISCCP data. *Atmos. Res.*, **37**, 133-146.

Carlson, T. N., 1969: Some remarks on African disturbances and their progress over the tropical Atlantic. *Mon. Wea. Rev.*, **97**, 716-726.

Chambers, L. H., B. A. Wielicki, and K. F. Evans, 1997: Independent pixel and two-dimensional estimates of Landsat-derived cloud field albedo. *J. Atmos. Sci.*, **54**, 1525-1532.

Chang, C.-P., 1970: Westward propagating cloud patterns in the tropical Pacific as seen from time-composite satellite photographs. *J. Atmos. Sci.*, **27**,133-137.

Chang, P., and S. G. H. Philander, 1994: A coupled ocean-atmosphere instability of relevance to the seasonal cycle. *J. Atmos. Sci.*, **51,** 3627-3648.

Cho, H.-R., and Y. Ogura, 1974: A relationship between cloud activity and the low-level convergence as observed in Read-Recker's composite easterly waves. *J. Atmos. Sci.*, **31,** 2058-2065.

Clark, J. H. E., 1993: Radiatively driven interactions between stratocumulus and synoptic waves. *J. Atmos. Sci.*, **50,** 2731-2743.

Clement, A., and R. Seager, 1999: Climate and the tropical oceans. *J. Climate*, **12**, 3383-3401.

Deardorff, J. W., 1980: Cloud top entrainment instability. *J. Atmos. Sci.*, **37**, 131-147.

Del Genio, A. D., M.-S. Yao, W. Kovari, and K. K. W. Lo, 1996: A prognostic cloud water parameterization for global climate models. *J. Climate*, **9**, 270-304.

Gilman, D. L., F. J. Fuglister, and J. M. Mitchell, Jr., 1963: On the power spectrum of "red noise". *J. Atmos. Sci.*, **20**, 182-184.

Gordon, C. T., A. Rosati, and R. Gudgel, 2000: Tropical sensitivity of a coupled model to specified ISCCP low clouds. *J. Climate*, **13**, 2239-2260.

Hack, J. J., W. H. Schubert, D. E. Stevens, and H.-C. Kuo, 1989: Response of the Hadley circulation to convective forcing in the ITCZ. *J. Atmos. Sci.*, **46**, 2957-2973.

Hahn, C. J., W. B. Rossow, and S. G. Warren, 2001: ISCCP cloud properties associated with standard cloud types identified in individual surface observations. *J. Climate*, **14**, 11-28.

Han, Q., W. B. Rossow, J. Chou and R. M. Welch, 1998: Global survey of the relationships of

cloud albedo and liquid water path with droplet size using ISCCP. *J. Climate*, **11**, 1516-1528.

Jakob, C., 1999: Cloud cover in the ECMWF reanalysis. *J. Climate*, **12**, 947-959.

Klein, S. A., and D. L. Hartmann, 1993: The seasonal cycle of low stratiform clouds. *J. Climate*, **6**, 1587-1606.

Klein, S. A., 1994: Large-scale variations in boundary layer cloud cover and their relationships to meteorological parameters. Ph. D Dissertation, University of Washington, 206pp.

Klein, S. A., D. L. Hartmann, and J. R. Norris, 1995: On the relationships among low-cloud structure, sea surface temperature, and atmospheric circulation in the summertime northeast Pacific. *J. Climate*, **8**, 1140-1155.

Klein, S. A., 1997: Synoptic variability of low-cloud properties and meteorological parameters in the subtropical trade wind boundary layer. *J. Climate*, **10**, 2018-2039.

Larson, K., D. L. Hartmann, and S. A. Klein, 1999: The role of clouds, water vapor, circulation, and boundary layer structure in the sensitivity of the tropical climate. *J. Climate*, **12**, 2359-2374.

Lau, N.-C., and M. W. Crane, 1995: A satellite view of the synoptic-scale organization of cloud properties in midlatitude and tropical circulation systems. *Mon. Wea. Rev.*, **123**, 1984-2006.

Lau, N.-C., and M. W. Crane, 1997: Comparing satellite and surface observations of cloud patterns in synoptic-scale circulation systems. *Mon. Wea. Rev.*, **125**, 3172-3189.

Leith, C. E., 1973: The standard error of time-average estimates of climatic means. *J. Appl. Meteor.*, **12**, 1066-1069.

Li, J.-F., M. Kohler, and C. R. Mechoso, 2000: The impact of improved stratocumulus cloud optical properties on a general circulation model. *Proc. 13th Int. Conf. on Clouds and Precipitation*, Vol. 2, Reno, Nevada, U.S.A., Int. Comm. Clouds and Precipitation, 311-314.

Ma, C.-C., C. R. Mechoso, A. W. Robertson, and A. Arakawa, 1996: Peruvian stratus clouds and the tropical Pacific circulation: A coupled ocean-atmosphere GCM study. *J. Climate*, **9**, 1635-1645.

Miller, R., 1997: Tropical thermostats and low cloud cover. *J. Climate*, **10**, 409-440.

Mitchell, T. P., and J. M. Wallace, 1992: The annual cycle in equatorial convection and sea surface temperature. *J. Climate*, **5**, 1140-1156.

Moeng, C.-H., W. R. Cotton, C. Bretheron, A. Chlond, M. Khairoutdinov, S. Krueger, W. S. Lewellen, M. K. MacVean, J. R. M. Pasquier, H. A. Rand, A. P. Siebesma, B. Stevens, and R. I. Sykes, 1996: Simulation of a stratocumulus-topped planetary boundary layer: Intercomparison among different numerical codes. *Bull. Amer. Meteor. Soc.*, **77**, 261-278.

Nicholls, S., 1984: The dynamics of stratocumulus: aircraft observations and comparisons with a mixed layer model. *Quart. J. Roy. Meteor. Soc.*, **110**, 783-820.

Norris, J. R., 1998: Low cloud type over the ocean from surface observations. Part I: Relationship to surface meteorology and the vertical distribution of temperature and moisture. *J. Climate*, **11**, 369-382.

Norris, J. R., and S. A. Klein, 2000: Low cloud type over the ocean from surface observations. Part III: Relationship to vertical motion and the regional surface synoptic environment. *J. Climate*, **13**, 245-256.

Pandolfo, L., 1993: Observational aspects of the low-frequency intraseasonal variability of the atmosphere in middle latitudes. *Adv. Geophys.*, **34**, 93-174.

Philander, S. G. H., D. Gu, D. Halpern, G. Lambert, N.-C. Lau, T. Li, and R. C. Pacanowski, 1996: Why the ITCZ is mostly north of the equator. *J. Climate*, **9**, 2958-2972.

Randall, D. A., 1980: Conditional instability of the first kind upside-down. *J. Atmos. Sci.*, **37**, 125-130.

Reed, R. J., D. C. Norquist, and E. E. Recker, 1977: The structure and properties of African wave disturbances as observed during Phase III of GATE. *Mon. Wea. Rev.*, **103**, 317-333.

Rind, D., and W. B. Rossow, 1984: The effects of physical processes on the Hadley circulation. *J. Atmos. Sci.*, **41**, 479-507.

Rossow, W. B., and A. A. Lacis, 1990: Global, seasonal cloud variations from satellite radiance measurements. Part II: Cloud properties and radiative effects. *J. Climate*, **3**, 1205-1253.

Rossow, W. B., and B. Cairns, 1995: Monitoring changes of clouds. *Climatic Change*, **31**, 305-

347.

Rossow, W. B., and R. A. Schiffer, 1999: Advances in understanding clouds from ISCCP. *Bull. Amer. Meteor. Soc.*, **80**, 2261-2287.

Rossow, W. B., A. W. Walker, and L. C. Garder, 1993: Comparison of ISCCP and other cloud amounts. *J. Climate*, **6**, 2394-2418.

Rossow, W. B., A. W. Walker, D. E. Beuschel, and M. D. Roiter, 1996: International Satellite Cloud Climatology Project (ISCCP) description of new cloud datasets. WMO/TD 737, World Climate Research Programme (ICSU and WMO), 115pp.

Rozendaal, M. A., C. B. Leovy, and S. A. Klein, 1995: An observational study of diurnal variations of marine stratiform cloud. *J. Climate*, **8**, 1795-1809.

Salby, M. L., 1996: Fundamentals of Atmospheric Physics. New York: Academic Press, 627pp.

Sarachik, E., 1978: Tropical sea surface temperature: An interactive one-dimensional atmosphere-ocean model. *Dyn. Atmos. Oceans*, **2,** 455-469.

Schubert, W. H., J. S. Wakefield, E. J. Steiner, and S. K. Cox, 1979: Marine stratocumulus convection. Part I: Governing equations and horizontally homogeneous solutions. *J. Atmos. Sci.*, **36**, 1286-1307.

Sengupta, S. K., R. M. Welch, M. S. Navar, T. A. Berendes, and D. W. Chen, 1990: Cumulus cloud field morphology and spatial patterns derived from high spatial resolution Landsat imagery. *J. Appl. Meteor.*, **29**, 1245-1267.

Simon, R. L., 1977: The summertime stratus over the offshore waters of California. *Mon. Wea. Rev.*, **105**, 1310-1314.

Slingo, J. M., 1980: A cloud parameterization scheme derived from GATE data for use with a numerical model. *Quart. J. Roy. Meteor. Soc.*, **106**, 747-770.

Stubenrauch, C. J., W. B. Rossow, F. Cheruy, A. Chedin, and N. A. Scott, 1999: Clouds as seen by satellite sounders (3I) and imagers (ISCCP). Part I: Evaluation of cloud parameters. *J. Climate*, **12**, 2189-2213.

Trenberth, K., 1991: Storm tracks in the southern hemisphere. *J. Atmos. Sci.*, **48**, 2159-2178.

Tselioudis, G., W. B. Rossow, and D. Rind, 1992: Global patterns of cloud optical thickness variation with temperature. *J. Climate*, **5**, 1484-1495.

Tselioudis, G., and W. B. Rossow, 1994: Global, multiyear variations of optical thickness with temperature in low and cirrus clouds. *Geophys. Res. Let.*, **21**, 2211-2214.

Tselioudis, G., Y.-C. Zhang, and W. B. Rossow, 2000: Cloud and radiation variations associated with northern midlatitude low and high sea level pressure regimes. *J. Climate*, **13**, 312-327.

Wang, J., W. B. Rossow, T. Uttal and M. Rozendaal, 1999: Variability of cloud vertical structure during ASTEX observed from a combination of rawinsonde, radar, ceilometer and satellite. *Mon. Wea. Rev.*, **127**, 2484-2502.

Warren, S. G., C. J. Hahn, J. London, R. M. Chevin, and R. L. Jenne, 1988: Global distribution of total cloud cover and cloud type amounts over the ocean. NCAR Tech. Note, NCAR/TN-317+STR, 42 pp. and 170 maps.

Weaver, C. P., and V. Ramanathan, 1997: Relationships between large-scale vertical velocity, static stability, and cloud radiative forcing over northern hemisphere extratropical oceans. *J. Climate*, **10**, 2871-2887.

Webb, M., C. A. Senior, S. Bony, and J.-J. Morcrette, 1999: Combining ERBE and ISCCP data to assess clouds in three climate models. *To be submitted.*

Welch, R. M., K. S. Kuo, B. A. Wielicki, S. K. Sengupta, and L. Parker, 1988: Marine stratocumulus cloud fields off the coast of southern California observed using LANDSAT imagery. Part I: Structural characteristics. *J. Appl. Meteor.*, **27**, 341-362.

Wylie, D., B. B. Hinton, and K. Kloesel, 1989: The relationship of marine stratus clouds to wind and temperature advection. *Mon. Wea. Rev.*, **117**, 2620-2625.

Yu, J.-Y., and C. R. Mechoso, 1999: Links between annual variations of Peruvian stratocumulus clouds and of SST in the eastern equatorial Pacific. *J. Climate*, **12**, 3305-3318.

Figure 1

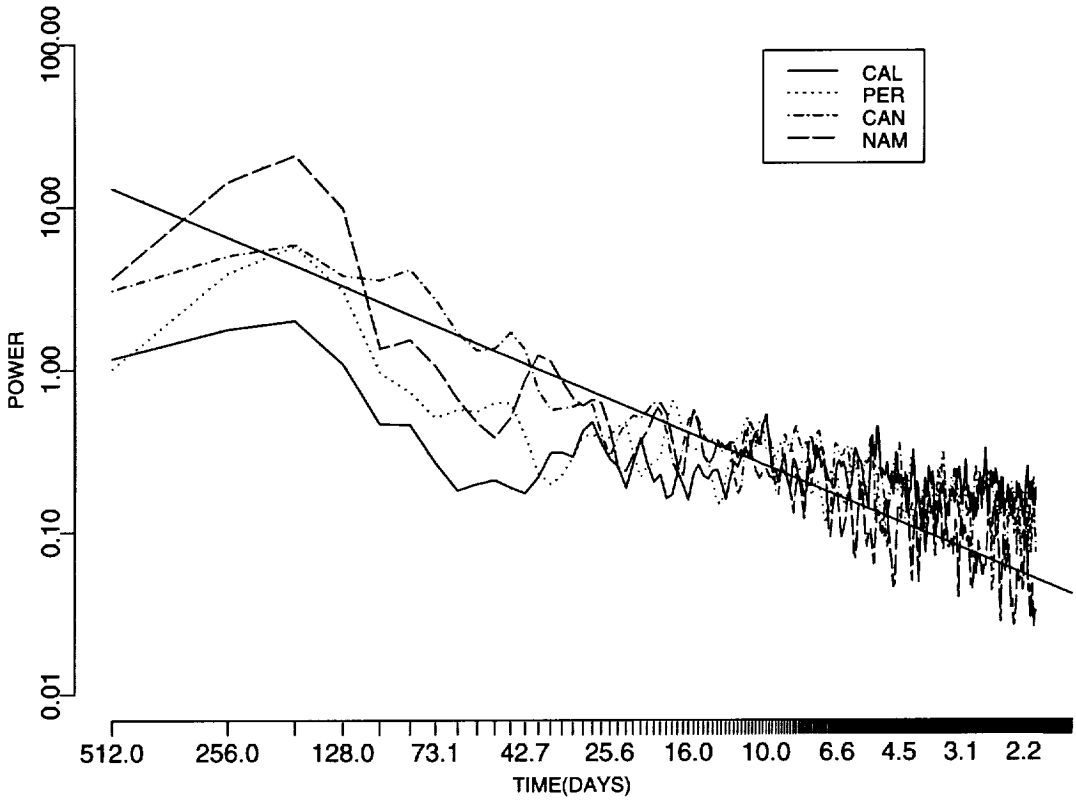
CAL
PER
CAN
NAM
POWER
100.00
10.00
1.00
0.10
0.01
512.0
256.0
128.0
73.1
42.7
25.6
16.0
10.0
6.6
4.5
3.1
2.2
TIME(DAYS)

Figure 2

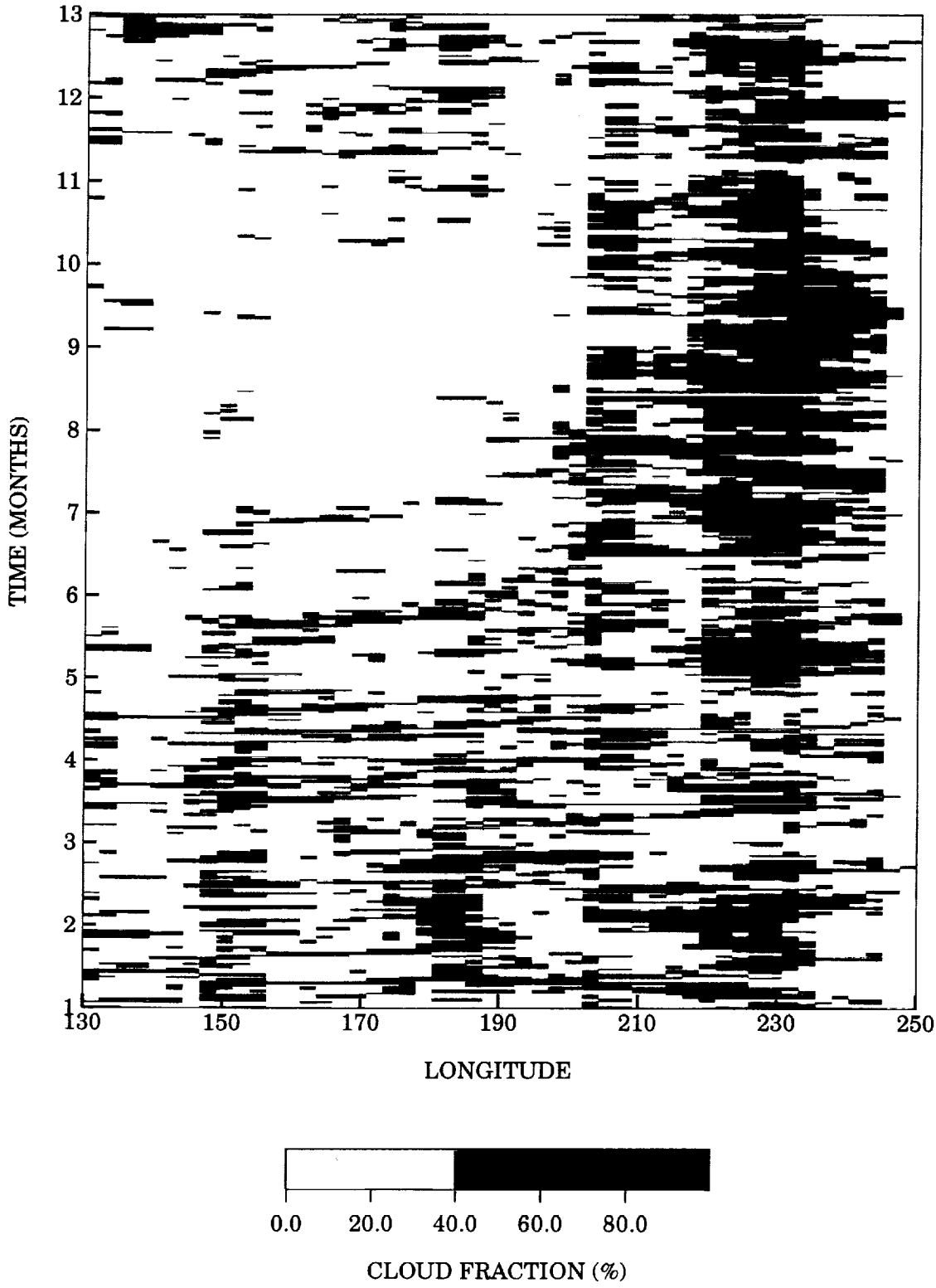
TIME (MONTHS)
13
12
11
10
9
8
7
6
5
4
3
2
1
130
150
170
190
210
230
250
LONGITUDE
0.0
20.0
40.0
60.0
80.0
CLOUD FRACTION (%)

Figure 3

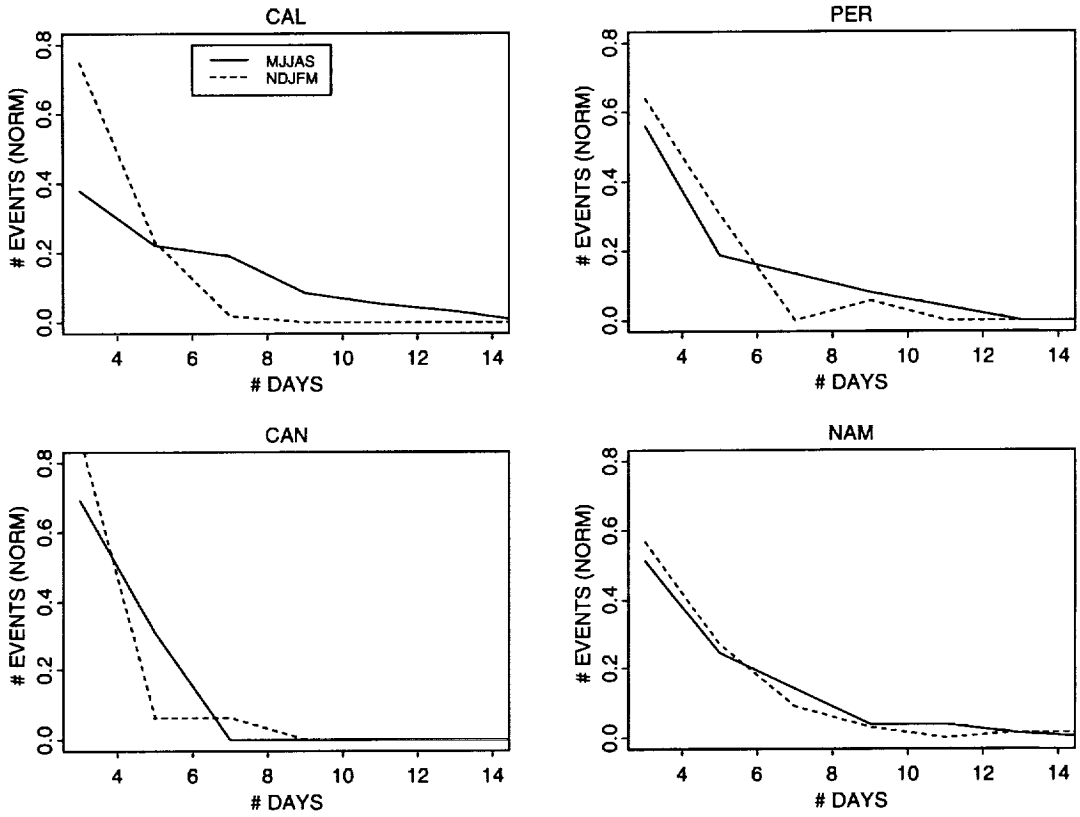
CAL
PER
CAN
NAM
MJJAS
NDJFM
EVENTS (NORM)
DAYS
0.0
0.2
0.4
0.6
0.8
4
6
8
10
12
14

Figure 4

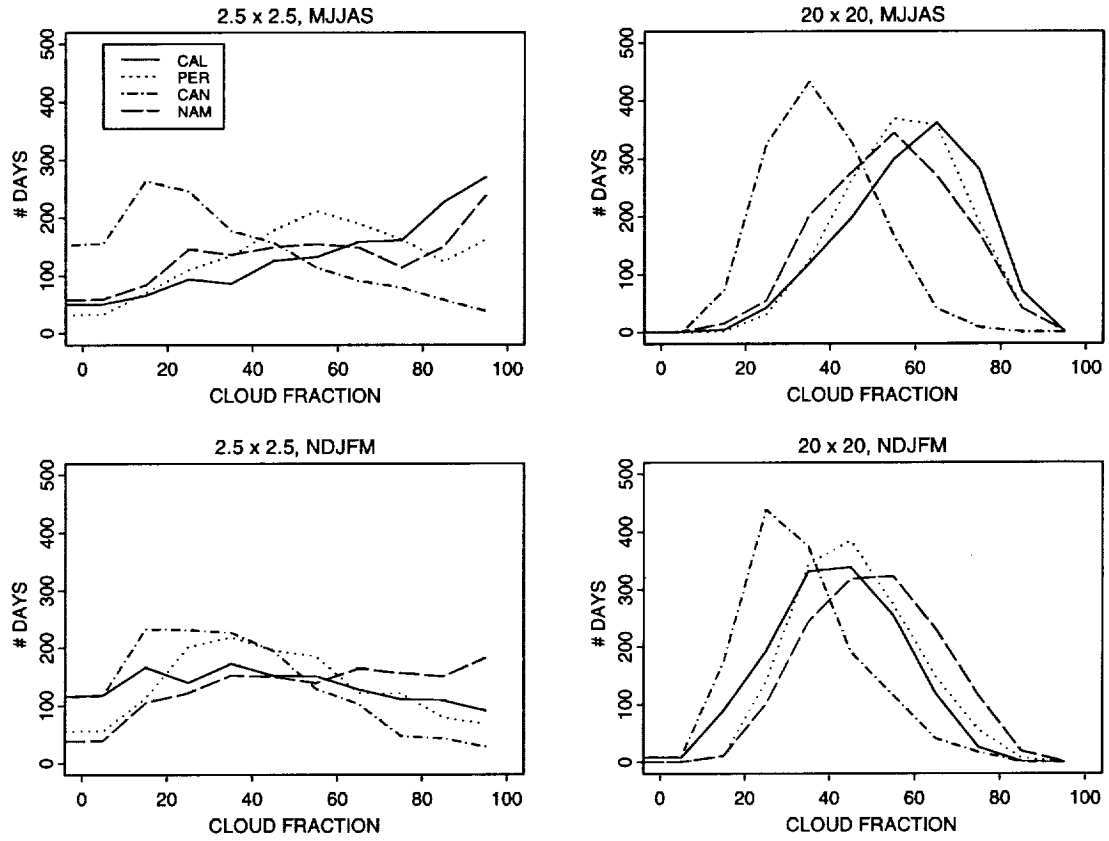
2.5 x 2.5, MJJAS
20 x 20, MJJAS
2.5 x 2.5, NDJFM
20 x 20, NDJFM
CAL
PER
CAN
NAM
DAYS
CLOUD FRACTION
0
100
200
300
400
500
0
20
40
60
80
100

Figure 5

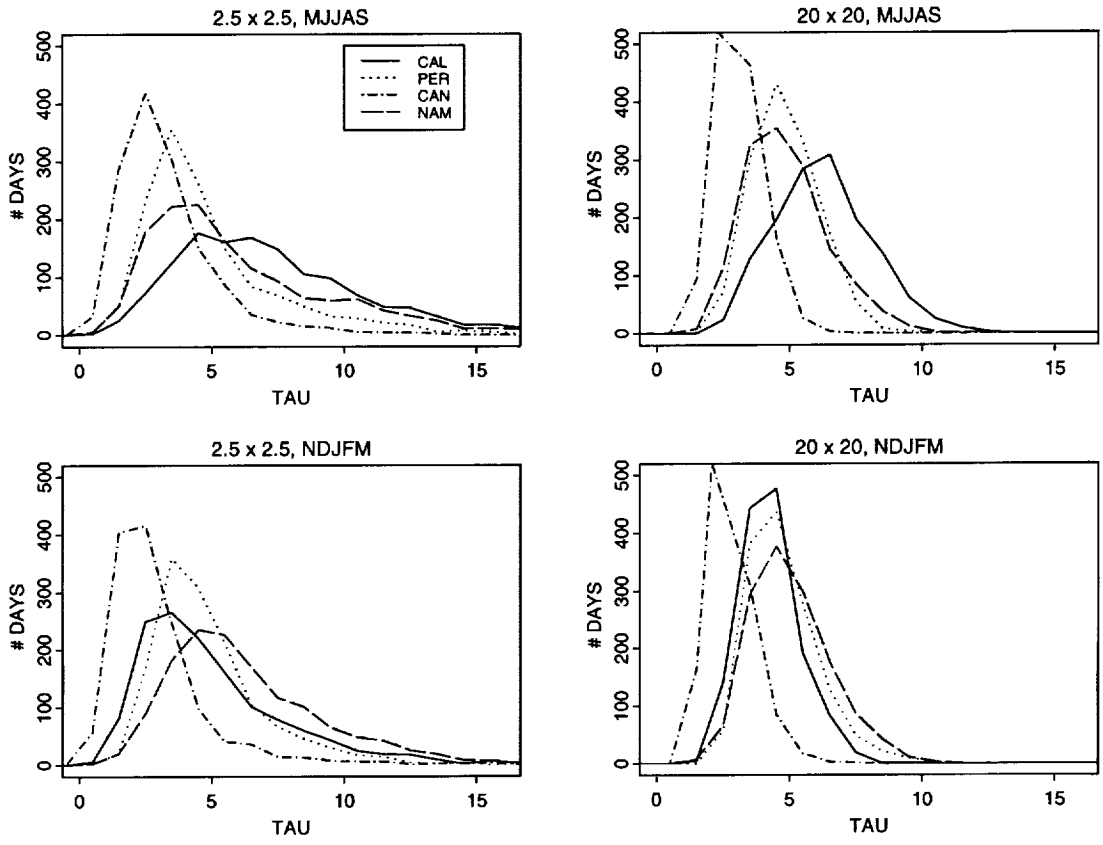
2.5 x 2.5, MJJAS
20 x 20, MJJAS
2.5 x 2.5, NDJFM
20 x 20, NDJFM
CAL
PER
CAN
NAM
DAYS
TAU
0
100
200
300
400
500
5
10
15

Figure 6

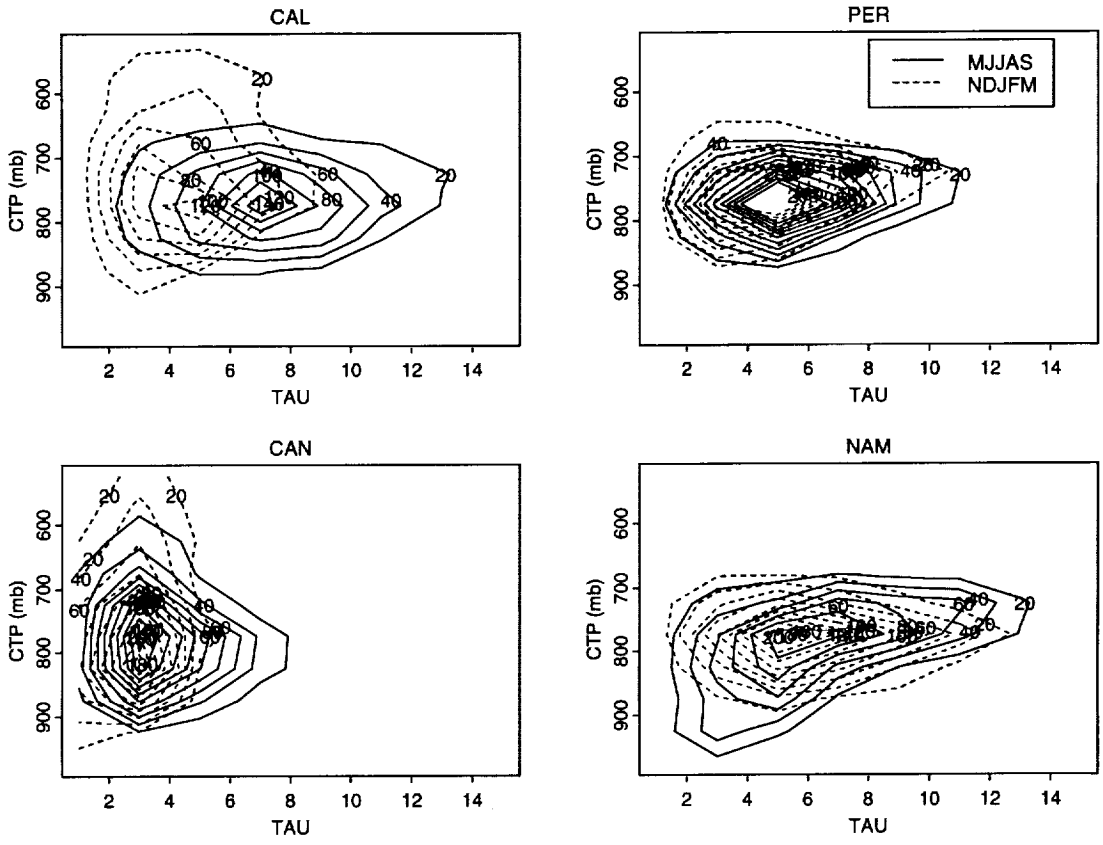
CAL
PER
CAN
NAM
MJJAS
NDJFM
CTP (mb)
TAU
600
700
800
900
2
4
6
8
10
12
14

Figure 7

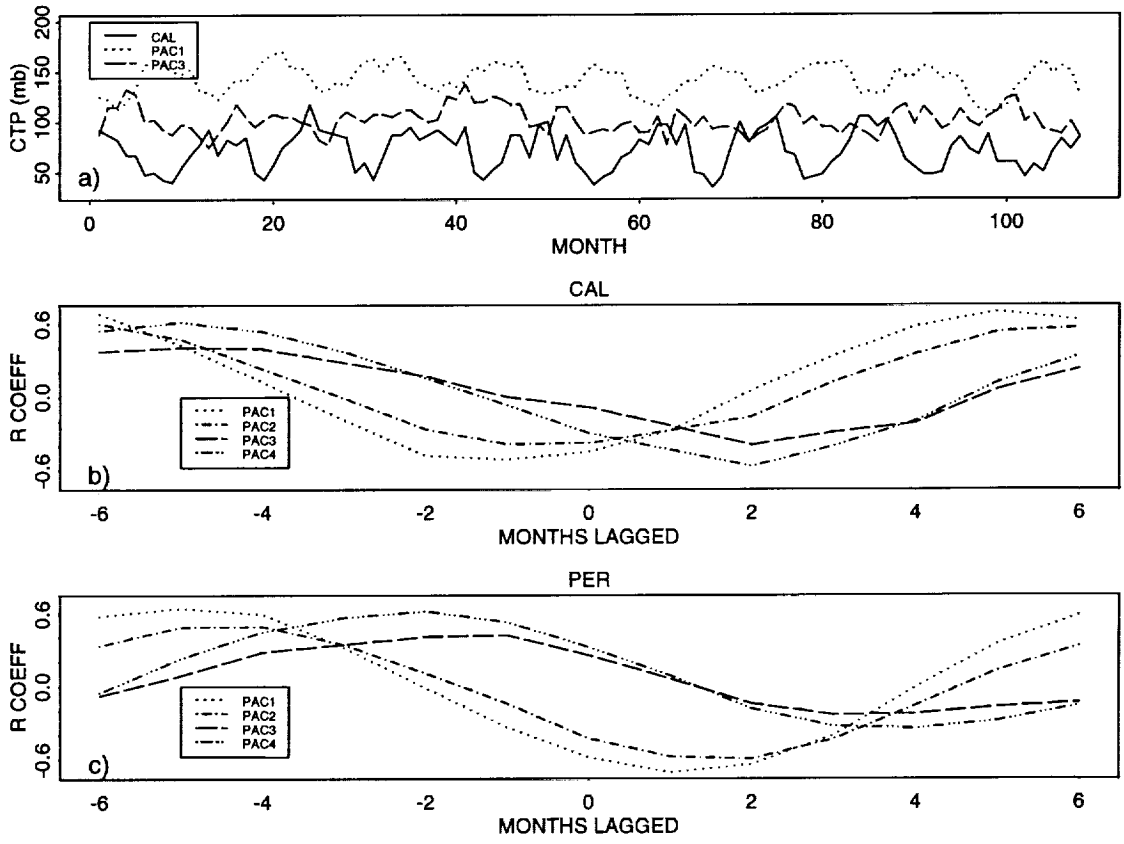
CAL
PAC1
PAC3
CTP (mb)
50
100
150
200
a)
0
20
40
60
80
100
MONTH
CAL
R COEFF
-0.6
0.0
0.6
PAC1
PAC2
PAC3
PAC4
b)
-6
-4
-2
0
2
4
6
MONTHS LAGGED
PER
R COEFF
-0.6
0.0
0.6
PAC1
PAC2
PAC3
PAC4
c)
-6
-4
-2
0
2
4
6
MONTHS LAGGED

Figure 8

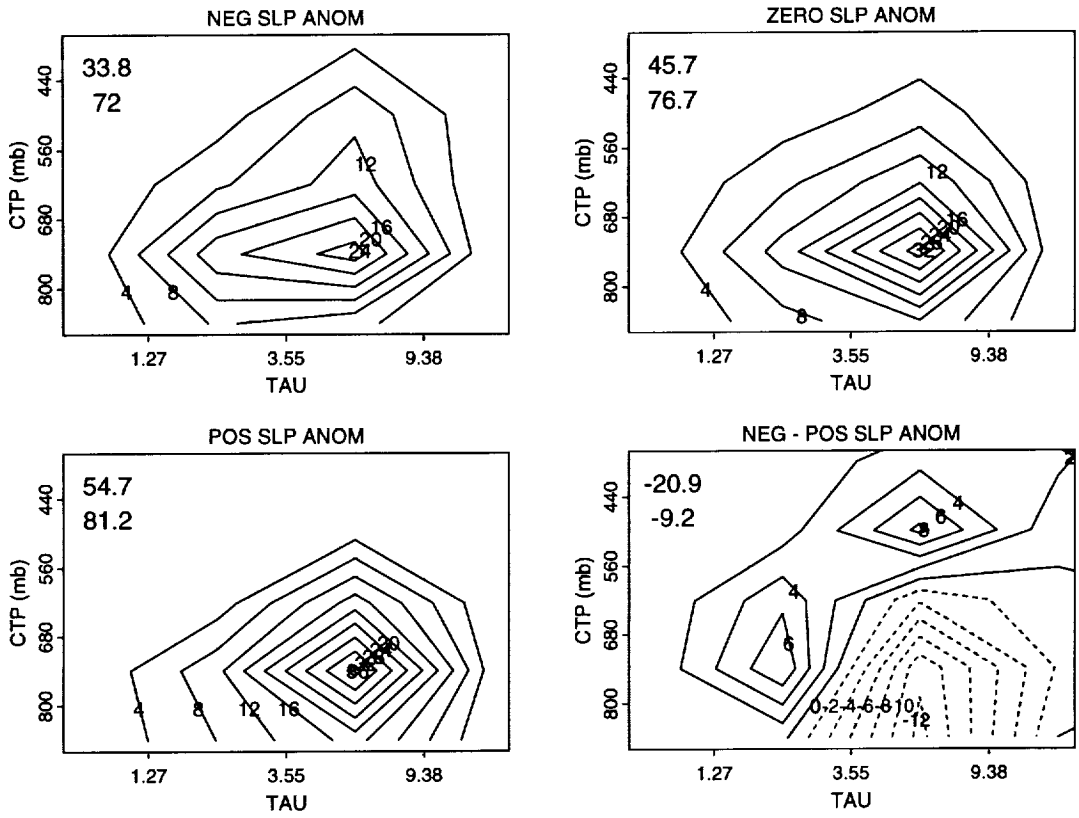
NEG SLP ANOM
33.8
72
ZERO SLP ANOM
45.7
76.7
POS SLP ANOM
54.7
81.2
NEG - POS SLP ANOM
-20.9
-9.2
CTP (mb)
440
560
680
800
1.27
3.55
9.38
TAU

Figure 9

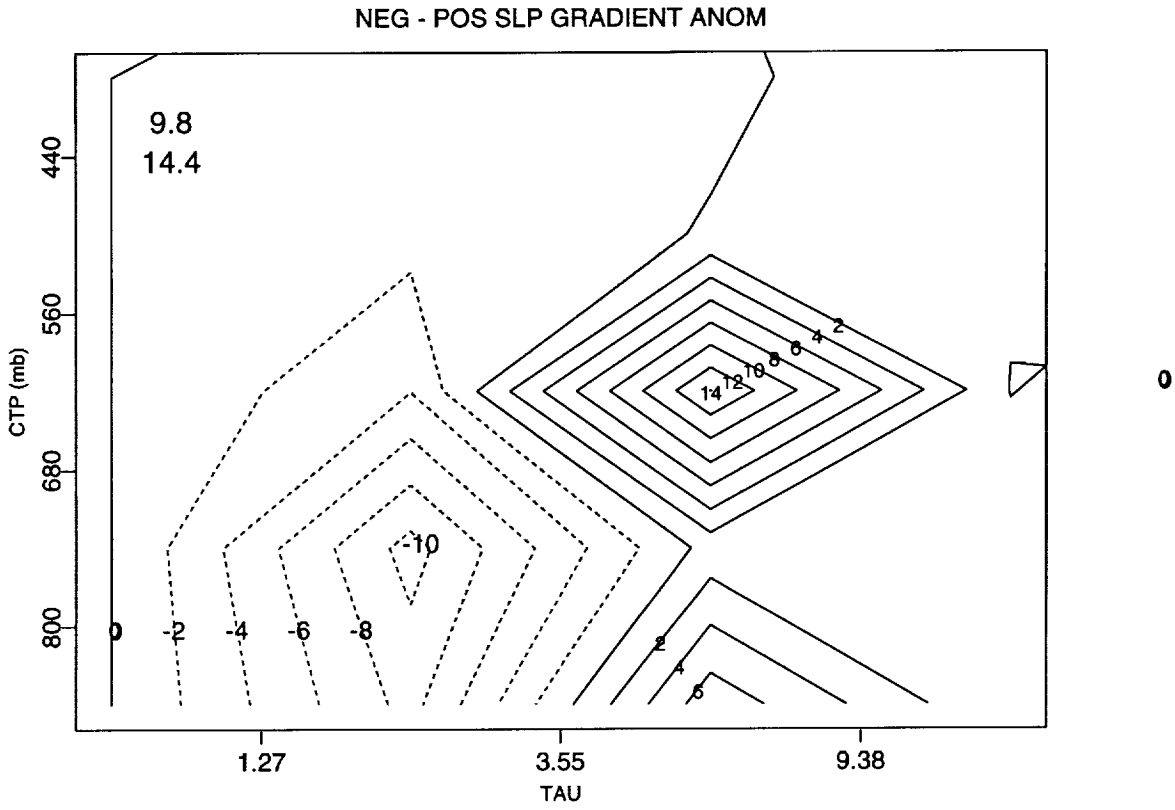
NEG - POS SLP GRADIENT ANOM
9.8
14.4
440
560
680
800
CTP (mb)
0
-2
-4
-6
-8
-10
2
4
6
8
10
12
14
1.27
3.55
9.38
TAU

Figure 10

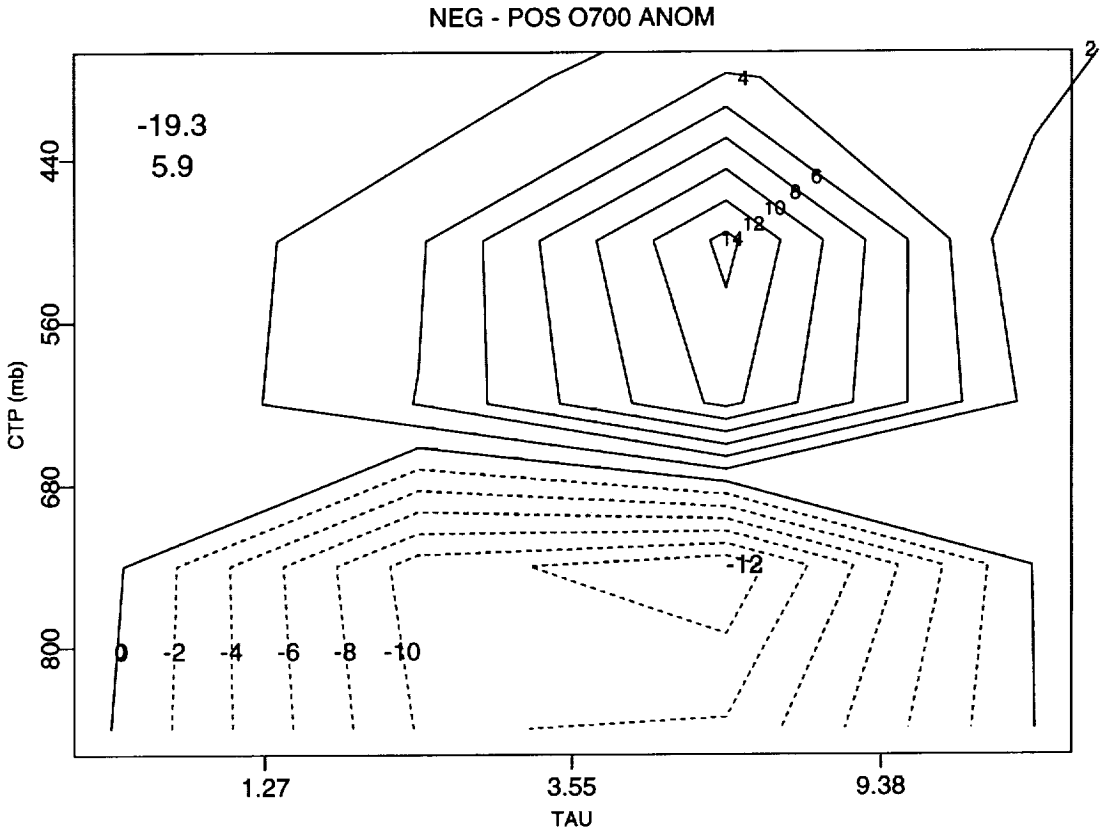
NEG - POS O700 ANOM
-19.3
5.9
2
4
6
8
10
12
14
-12
0
-2
-4
-6
-8
-10
440
560
680
800
CTP (mb)
1.27
3.55
9.38
TAU

Figure 11

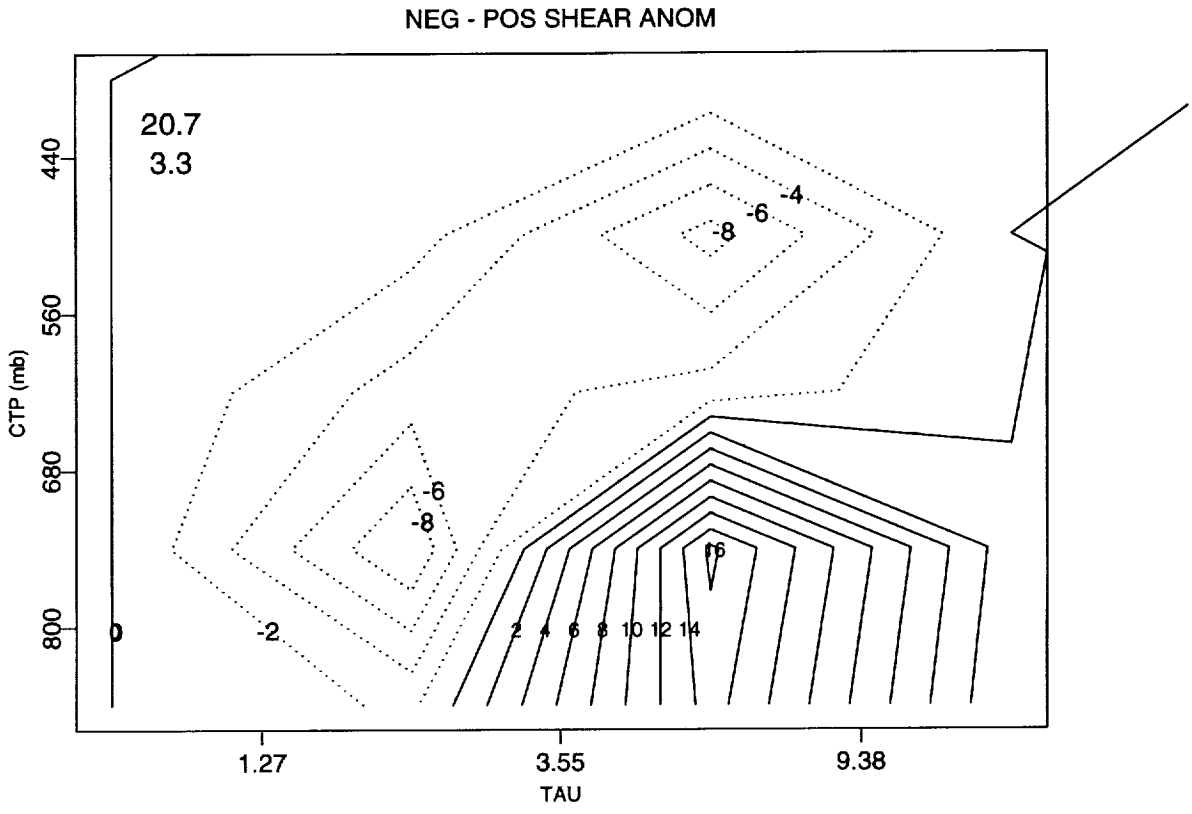
NEG - POS SHEAR ANOM
20.7
3.3
-4
-6
-8
-6
-8
-2
2 4 6 8 10 12 14
440
560
680
800
CTP (mb)
1.27
3.55
9.38
TAU

Figure 12

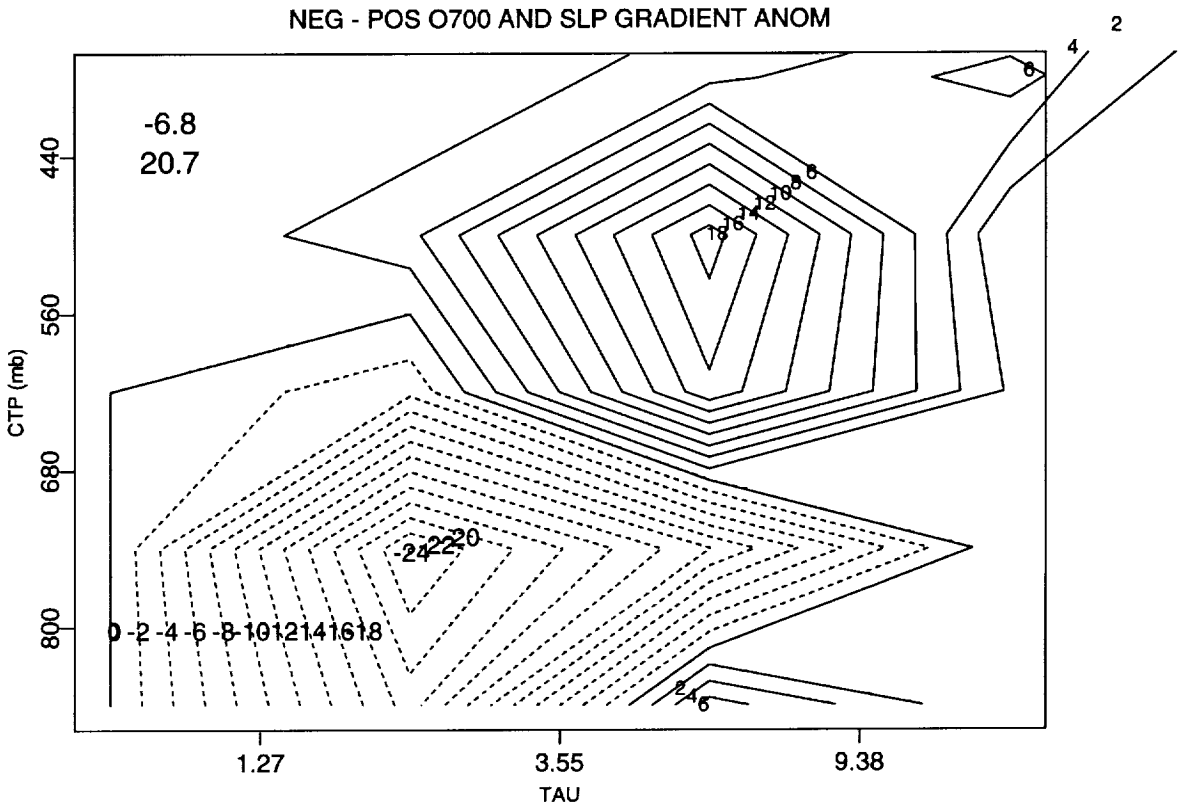
NEG - POS O700 AND SLP GRADIENT ANOM
-6.8
20.7
CTP (mb)
440
560
680
800
1.27
3.55
9.38
TAU

Figure 13

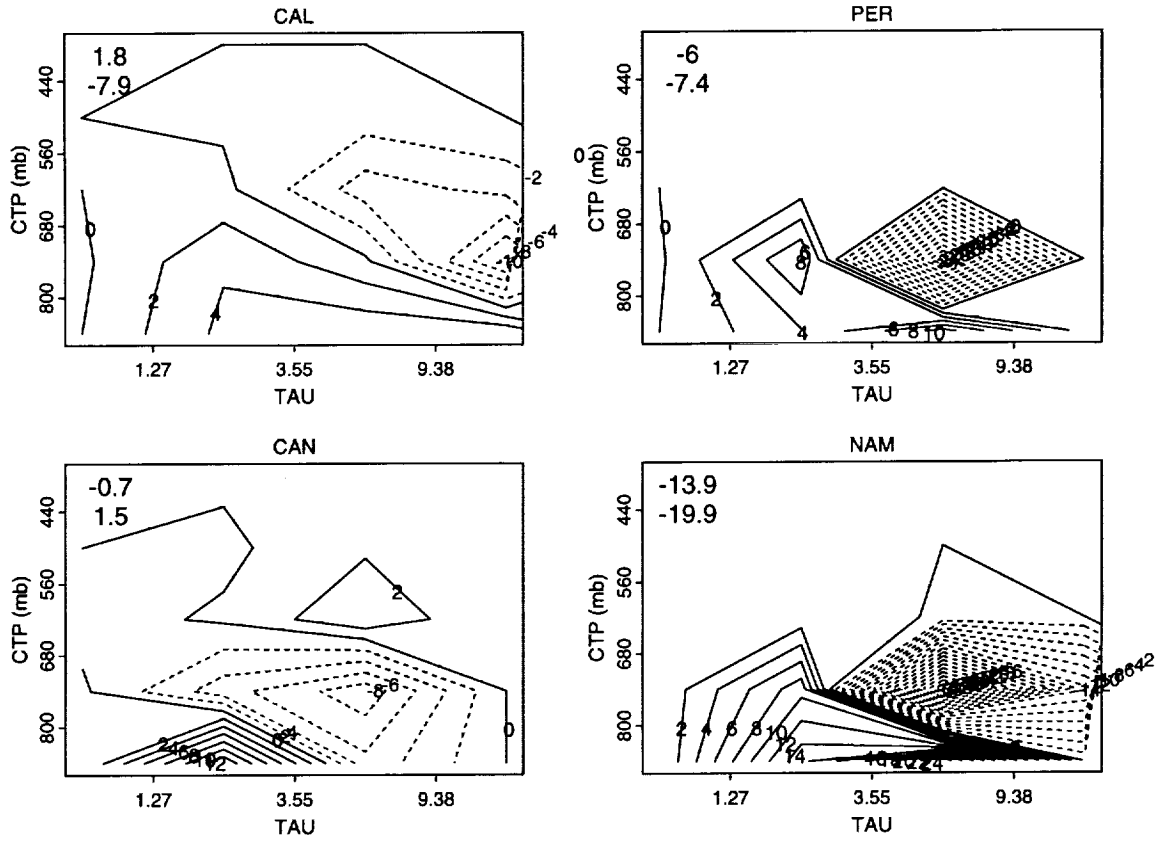
CAL
1.8
-7.9
PER
-6
-7.4
CAN
-0.7
1.5
NAM
-13.9
-19.9
CTP (mb)
440
560
680
800
1.27
3.55
9.38
TAU

Figure 14

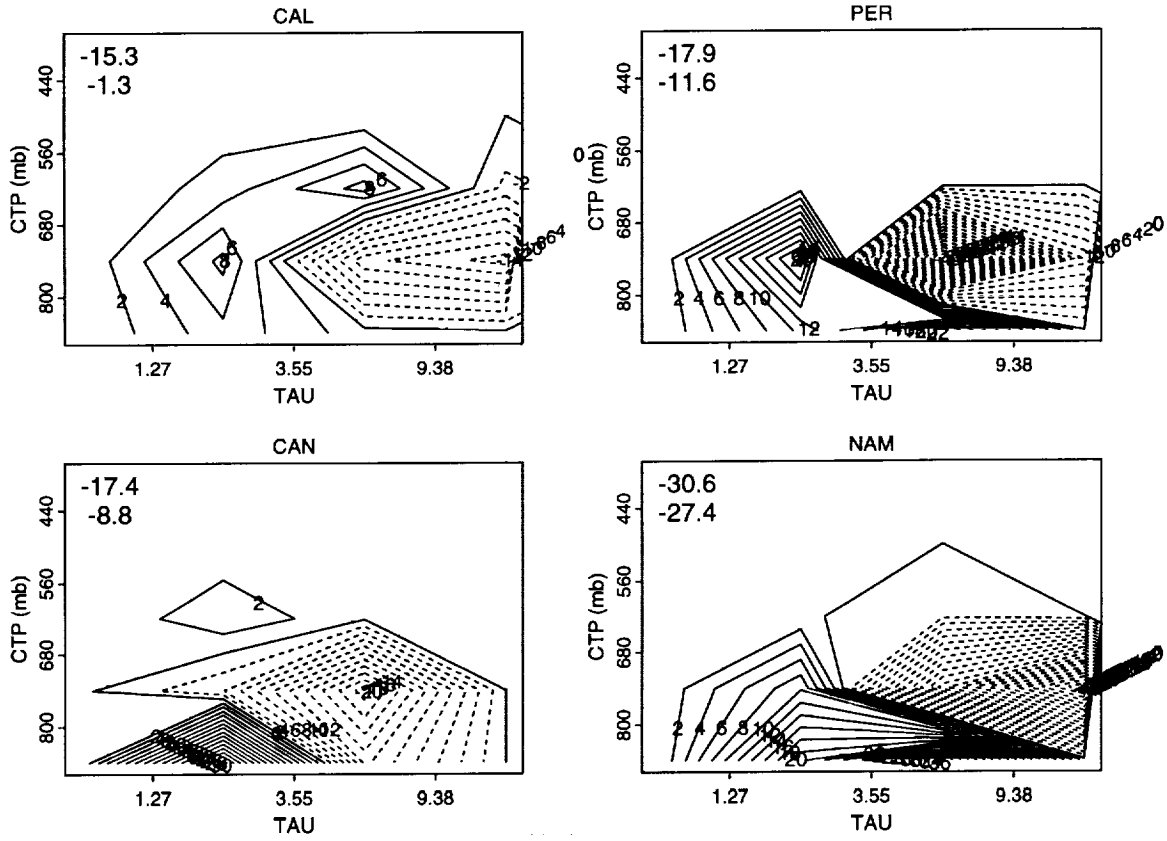
CAL
-15.3
-1.3
PER
-17.9
-11.6
CAN
-17.4
-8.8
NAM
-30.6
-27.4
CTP (mb)
440
560
680
800
1.27
3.55
9.38
TAU

Figure 15

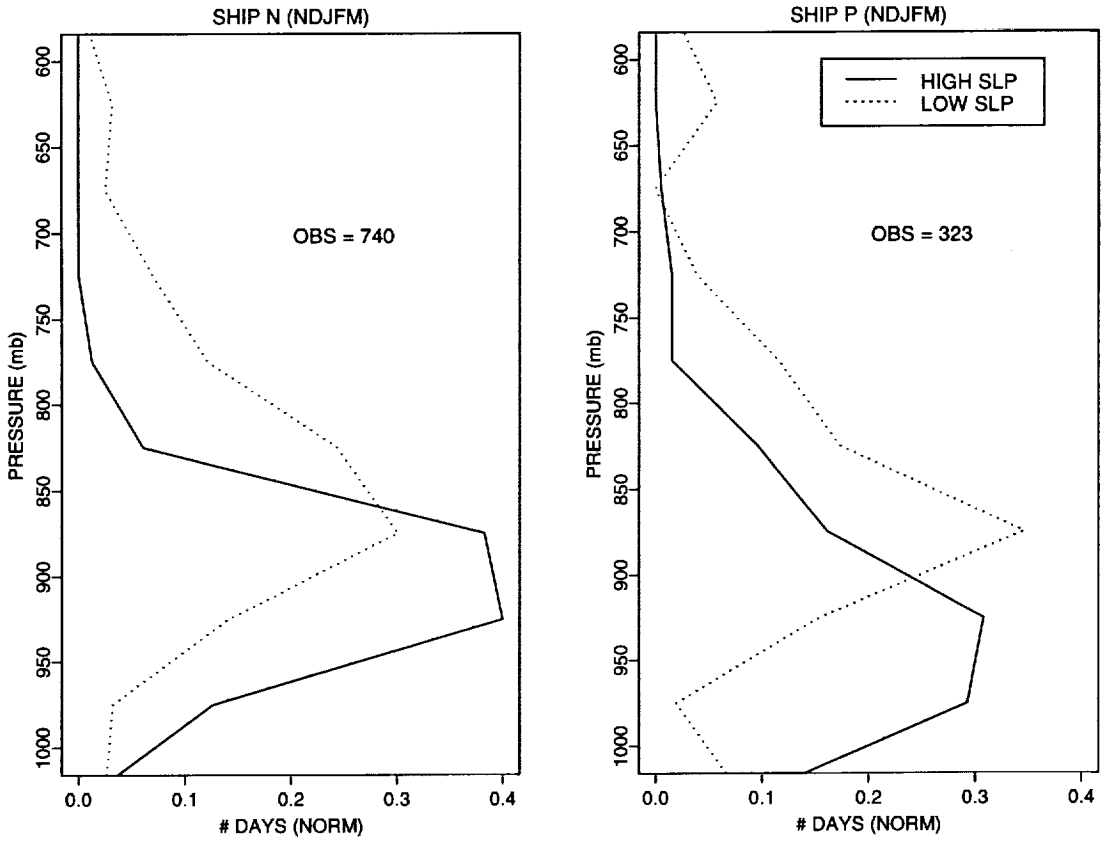
SHIP N (NDJFM)
OBS = 740
PRESSURE (mb)
600
650
700
750
800
850
900
950
1000
0.0
0.1
0.2
0.3
0.4
DAYS (NORM)
SHIP P (NDJFM)
HIGH SLP
LOW SLP
OBS = 323
PRESSURE (mb)
DAYS (NORM)

Figure 16

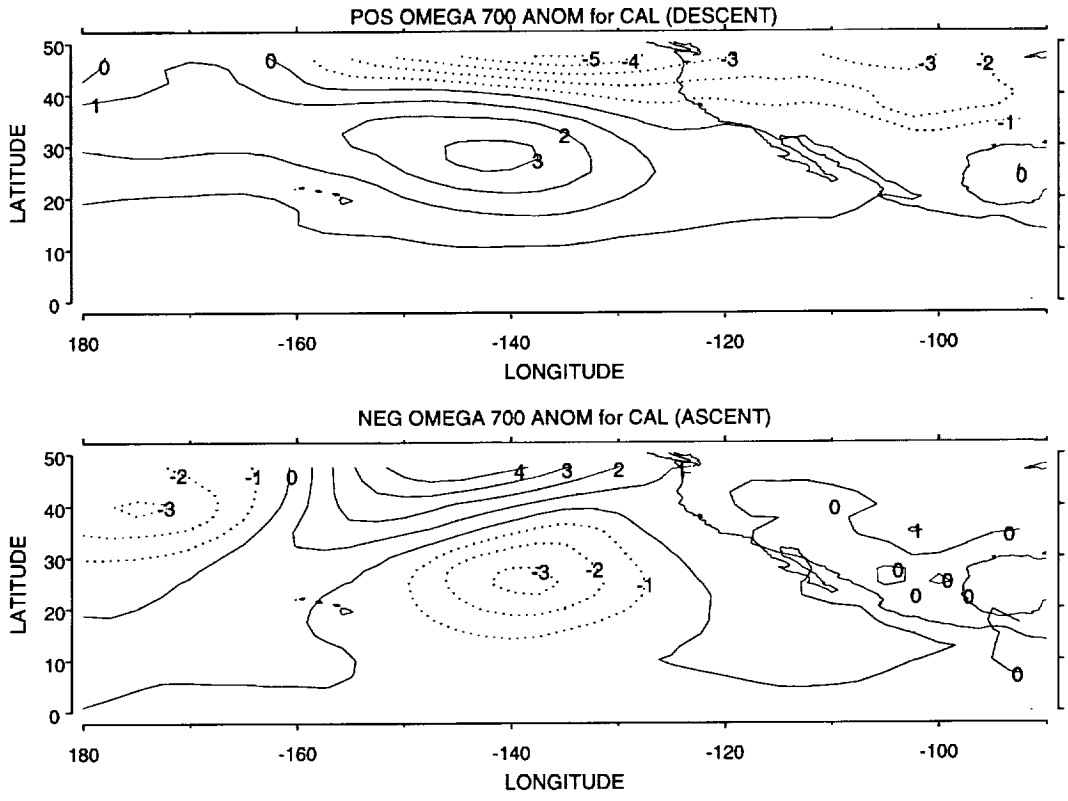
POS OMEGA 700 ANOM for CAL (DESCENT)
LATITUDE
LONGITUDE
50
40
30
20
10
0
180
-160
-140
-120
-100
NEG OMEGA 700 ANOM for CAL (ASCENT)
LATITUDE
LONGITUDE

Figure 17

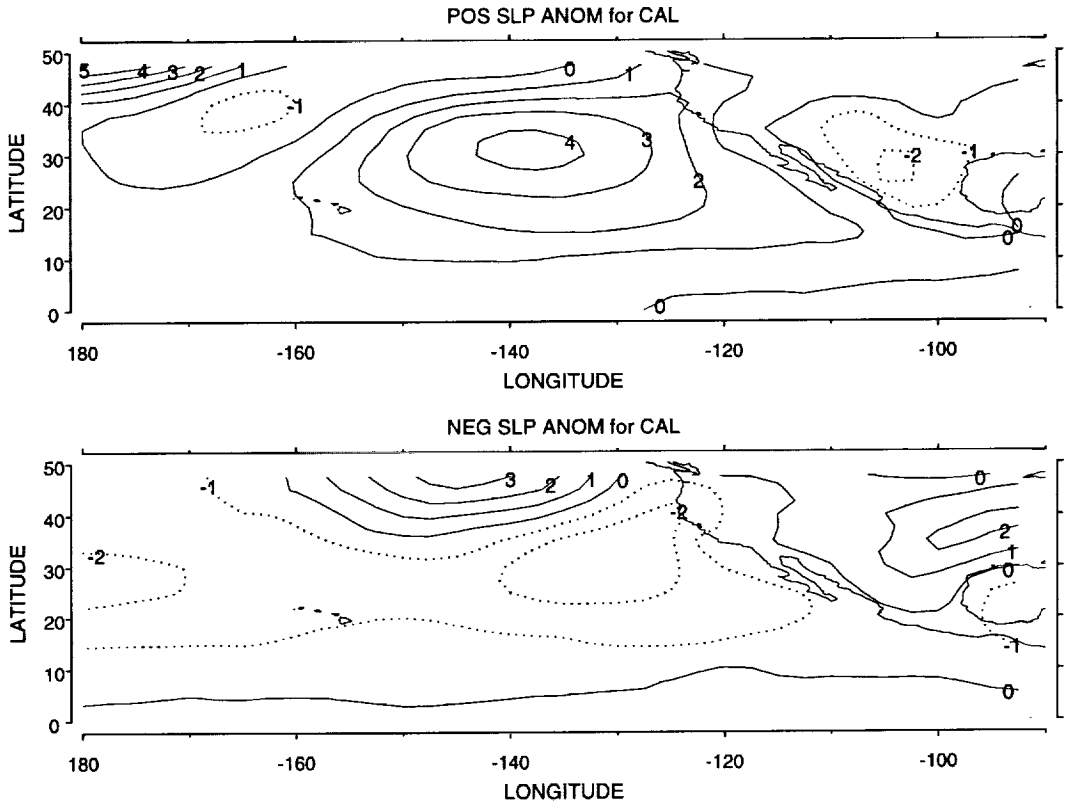
POS SLP ANOM for CAL
LATITUDE
LONGITUDE
50
40
30
20
10
0
180
-160
-140
-120
-100
NEG SLP ANOM for CAL
LATITUDE
LONGITUDE

Figure 18

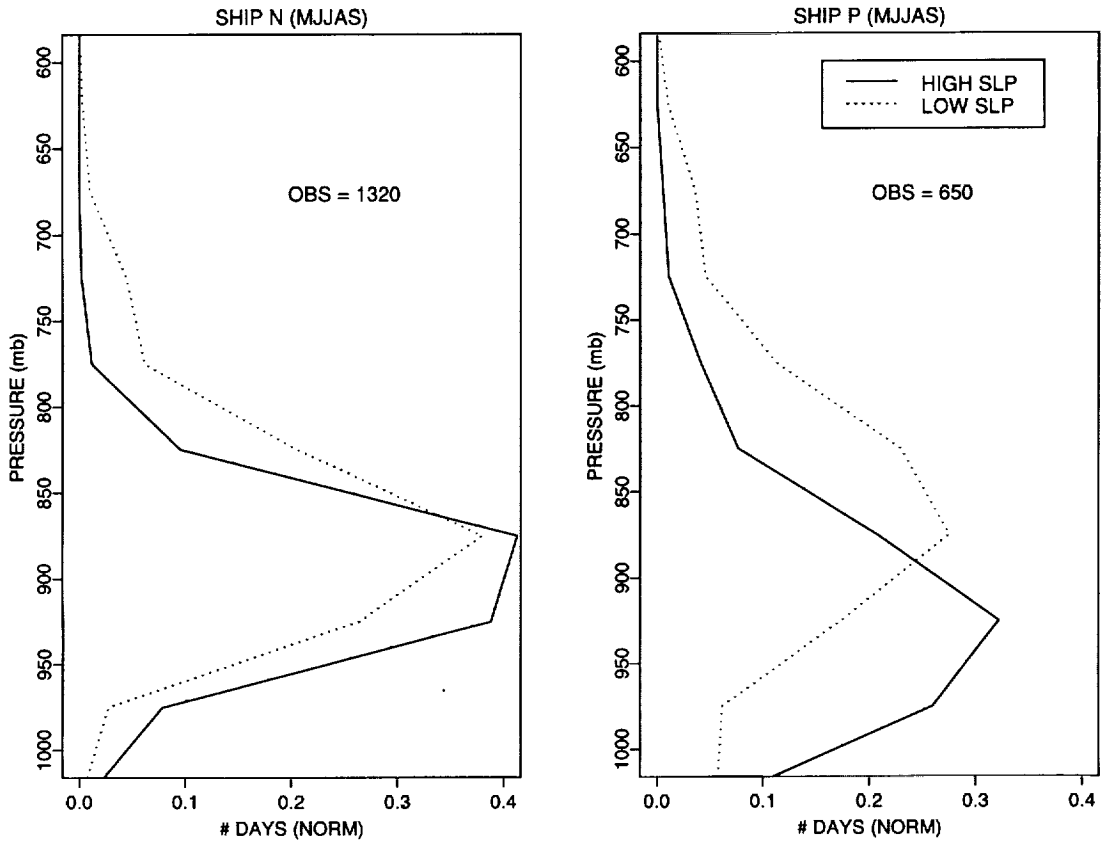
SHIP N (MJJAS)
OBS = 1320
PRESSURE (mb)
600
650
700
750
800
850
900
950
1000
0.0
0.1
0.2
0.3
0.4
DAYS (NORM)
SHIP P (MJJAS)
HIGH SLP
LOW SLP
OBS = 650
PRESSURE (mb)
DAYS (NORM)